

CoPATCH: ZERO-SHOT REFERRING IMAGE SEGMENTATION BY LEVERAGING UNTAPPED SPATIAL KNOWLEDGE IN CLIP

Na Min An¹ Inha Kang¹ Minhyun Lee² Hyunjung Shim^{1*}

¹Korea Advanced Institute of Science and Technology (KAIST)

²Samsung Electronics

{naminan, rkswlsj13, kateshim}@kaist.ac.kr

mh315.lee@samsung.com

ABSTRACT

Spatial grounding is crucial for referring image segmentation (RIS), where the goal of the task is to localize an object described by language. Current foundational vision-language models (VLMs), such as CLIP, excel at aligning images and text but struggle with understanding spatial relationships. Within the language stream, most existing methods often focus on the primary noun phrase when extracting local text features, undermining contextual tokens. Within the vision stream, CLIP generates similar features for images with different spatial layouts, resulting in limited sensitivity to spatial structure. To address these limitations, we propose CoPATCH, a zero-shot RIS framework that leverages internal model components to enhance spatial representations in both text and image modalities. For language, CoPATCH constructs hybrid text features by incorporating context tokens carrying spatial cues. For vision, it extracts patch-level image features using our novel path discovered from intermediate layers, where spatial structure is better preserved. These enhanced features are fused into a clustered image-text similarity map, CoMap, enabling precise mask selection. As a result, CoPATCH significantly improves spatial grounding in zero-shot RIS across RefCOCO, RefCOCO+, RefCOCOg, and PhraseCut (+ 2–7 mIoU) without requiring any additional training. Our findings underscore the importance of recovering and leveraging the untapped spatial knowledge inherently embedded in VLMs, thereby paving the way for opportunities in zero-shot RIS.

1 INTRODUCTION

Understanding spatial concepts is a fundamental cognitive ability that enables humans to interact with complex environments for real-life tasks (Wolbers & Hegarty, 2010). While humans naturally acquire spatial grounding ability (Wolbers & Hegarty, 2010; Piaget, 1952; Newcombe & Huttenlocher, 2000), current vision-language models (VLMs) still face significant challenges in this area. In particular, CLIP (Radford et al., 2021), one of the most widely used pretrained foundational VLMs, shows limited ability to perform even basic spatial or positional understanding (Tong et al., 2024; Tang et al., 2023; Peng et al., 2024; Kamath et al., 2023; Du et al., 2024; Chatterjee et al., 2024; Huang et al., 2023). This limitation is especially critical in real-world applications that rely heavily on fine-grained spatial grounding, such as robotic object manipulation (Billard & Kragic, 2019; Jang et al., 2006) and autonomous driving (Chen et al., 2024; Kim et al., 2024).

A particularly demanding testbed for spatial grounding is *zero-shot* referring image segmentation (RIS). In this task, the model needs to accurately segment the object *referred* by a natural language expression, without any task-specific training. This requires a pretrained CLIP to comprehend both the semantic meaning and the spatial location of the referred object (Subramanian et al., 2022; Yu et al., 2023; Suo et al., 2023; Wang et al., 2025; Liu & Li, 2025; Ni et al., 2023; Han et al.,

*Corresponding author

¹Code available at <https://github.com/kaist-cvml/copatch>.

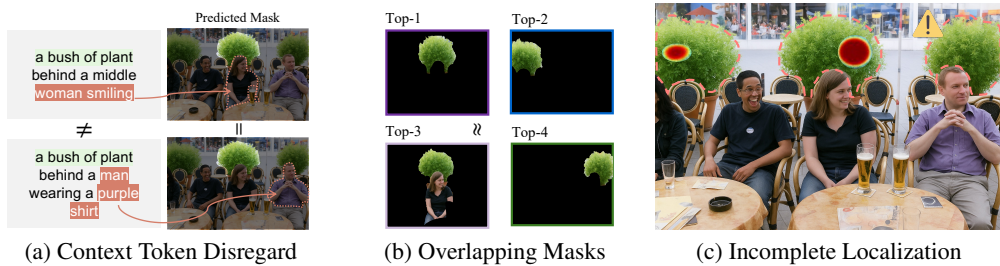


Figure 1: **Limitations of existing zero-shot RIS approaches.** Prior works lack in (a) incorporating contexts containing important cues for local-level text feature extraction, (b) filtering out top masks that may contain overlapping contents, and (c) spatially grounding all the target objects.

2024; Lüddecke & Ecker, 2022). The challenge becomes even more significant when multiple similar objects appear in different locations (Nagaraja et al., 2016; Mao et al., 2016; Wu et al., 2020) (Figure 1). Although the CLIP-based methods have made significant progress in aligning visual and textual semantics (An et al., 2025a), they continue to struggle with precise spatial grounding.

More specifically, existing zero-shot RIS approaches fail to encode spatial information via original feature extraction pathways for both texts and images. On the text side, their focus is on the primary noun phrase when extracting local-level text features. However, this could leave out important cues, namely, *context tokens*, that may appear after the primary noun chunk. This often leads to identical mask outputs for semantically different expressions, as shown in Figure 1a. On the image side, previous methods directly use the original CLIP image features, discarding *spatial layout* information maintained until the final layer. As a result, masked images with similar, overlapping semantics are selected in the top candidate masks (Figure 1b), reducing the reliability of the final mask selection process. These limitations underscore the need to leverage untapped model components to enhance zero-shot RIS ability for CLIP.

In this work, we present COPATCH, a training-free framework that unlocks the underexplored spatial understanding ability of CLIP for RIS. Our approach has two main components: First, we construct hybrid text features that incorporate *context tokens* carrying useful spatial cues. This textual guidance enables the model to capture subtle spatial distinctions of the same object names in referring expressions. Second, we devise an expressive *patch-level spatial map* through a newly identified pathway in CLIP’s visual encoder. This is motivated by our observation that the intermediate layers of the visual encoder can better preserve spatial information than the last layer. By combining these two sources, we generate a context-aware spatial map, CoMap, which reranks top candidate masks with greater spatial precision.

The novelty of COPATCH lies in its ability to enhance both text and image modalities without any additional training. Unlike gradient-based (Selvaraju et al., 2016) (Figure 1c) or attention-based (Li et al., 2023; Bousselham et al., 2024) localization methods, our approach is computationally efficient while offering stronger zero-shot spatial grounding. This shows that precise zero-shot segmentation can be achieved not by redesigning models or costly fine-tuning, but by strategically leveraging the underused capacities already present in pretrained foundational models.

To summarize, our contributions are as follows: 1) **Novel pathway for informative spatial map generation.** We discover a new computation-efficient pathway in CLIP’s visual encoder. This enables the extraction of a context-aware spatial map, CoMap, with a single forward pass without recomputations. 2) **Effective mask scoring strategy.** We propose a novel scoring framework that leverages CoMap to effectively rerank top candidate masks, ensuring that the most semantically aligned, non-overlapping masks are retained. This significantly improves the reliability of the final mask selection process. 3) **SoTA zero-shot RIS performances.** Our proposed COPATCH achieves mIoU scores of 55.62, 55.38, and 54.08, in the RefCOCO (Nagaraja et al., 2016), RefCOCO+ (Nagaraja et al., 2016), and RefCOCOg (Mao et al., 2016) test sets, outperforming the current SoTA (Liu & Li, 2025) by +4.03p, +2.01p, and +4.95p. We hope our work paves the future work in proposing various zero-shot RIS methods by extracting enhanced inherent spatial knowledge from VLMs.

2 RELATED WORKS

Referring Image Segmentation. Referring Image Segmentation (RIS) aims to segment image regions described by text expressions. Early supervised methods rely on mask annotations to learn dense cross-modal correspondences. LAVT (Yang et al., 2022) introduces a language-aware vision transformer that employs early fusion and stacked cross-modal attention for feature refinement. CRIS (Wang et al., 2022b) adds a CLIP-driven decoder trained with a contrastive loss to enhance text-pixel alignment. RISCLIP (Kim et al., 2023b) adapts CLIP features through parameter-efficient fusion layers. ETRIS (Xu et al., 2023) inserts lightweight adapter modules between frozen CLIP encoders, achieving competitive accuracy with few additional parameters. Prompt-Driven RIS (Shang et al., 2024) injects instance-aware prompts into CLIP and refines masks using SAM (Kirillov et al., 2023). UniNeXt (Lin et al., 2023) aims for unification, integrating RIS with other vision tasks using shared transformer heads.

To mitigate the high cost of pixel-level annotations, weakly-supervised methods emerged, relying only on image-text pairs. Techniques include enforcing text-region consistency (Strudel et al., 2022). Moreover, the prior approaches maintain intra-chunk semantic coherence (Lee et al., 2023a), connect regions to linguistic cues via shatter-and-gather mechanisms (Kim et al., 2023a), and mine text-region interactions (Liu et al., 2023). Pseudo-supervised approaches, such as Pseudo-RIS (Yu et al., 2024), further bridge the gap by leveraging foundation models to generate high-quality pseudo-masks for training, eliminating the need for manually generating ground-truth masks.

Zero-shot Referring Image Segmentation. Recent zero-shot RIS methods leverage pretrained vision-language models (VLMs) to avoid costly pixel-wise annotations and training with the following standard pipeline: 1) generating candidate masks using a pretrained segmentation model (Kirillov et al., 2023; Cheng et al., 2022; Liang et al., 2023; Wang et al., 2022a), 2) computing a similarity score between each masked image and the referring expression, and 3) selecting the mask with the highest score as output. To improve zero-shot mask scoring (the second stage), various methods have been proposed: ReCLIP (Subramanian et al., 2022) uses a heuristic spatial relation resolver to score the isolated mask proposals by calculating the probability for each noun chunk node. CLIPSeg (Lüddecke & Ecker, 2022) segments the image using a set of prompts at inference time. Several fully training-free comparison baseline methods include: a) **Region Token** (Li et al., 2022a) method calculates the cosine similarity between spatial feature per pixel and text embeddings for extracting a final mask (Suo et al., 2023). b) **CLIPSurgery** (Li et al., 2023) and c) **Cropping** use the average activation score (Suo et al., 2023) and cosine similarity between cropped image features and text features (Yu et al., 2023) for scoring masks. d) **Global-Local** uses the cosine similarity between global-local image features and text features (Yu et al., 2023). e) **TAS** augments the mask scores using features of negative texts generated by an external captioner, BLIP-2. f) **HybridGL** (Liu & Li, 2025) proposes a new image/text feature extraction strategy by fusing global image features into local image features (G2L) and using the cosine similarity between the hybrid G2L image and global-local text features.

Our method aligns more similarly to several recent zero-shot RIS methods that use a spatial map as a guide for the mask scoring step. For instance, **Ref-Diff** (Ni et al., 2023) uses a diffusion model to generate their own spatial map and uses a weighted sum of images multiplied by the positional bias matrix and mask proposals. **CaR** (Sun et al., 2024) uses Grad-CAM as the spatial map to generate mask proposals and filters the masks using similarity between each query (that may contain irrelevant texts) and masked images. **IteRPrimE** (Wang et al., 2025) uses an interpolated Grad-CAM heatmap generated using the primary word to guide the model for the candidate mask selection. **HybridGL** (Liu & Li, 2025) uses pretrained GEM (Bousselham et al., 2024) as the spatial map and reranks the initial mask scores with their proposed spatial *relation* and *coherence* guidance. Our CoPATCH is distinguished from HybridGL because it uses different spatial *relation* guidance using our proposed spatial map, but incorporates their spatial *coherence* method to boost the final performance (see Method and Ablation Study in Sections 3.2 and 4.3).

3 COPATCH: CONTEXT TOKEN-PATCH LEVEL EMBEDDING SYNERGY

Our proposed framework, CoPATCH, is designed to recover CLIP’s latent spatial grounding ability by jointly enhancing text and image representations (Figure 2). This framework has two essential

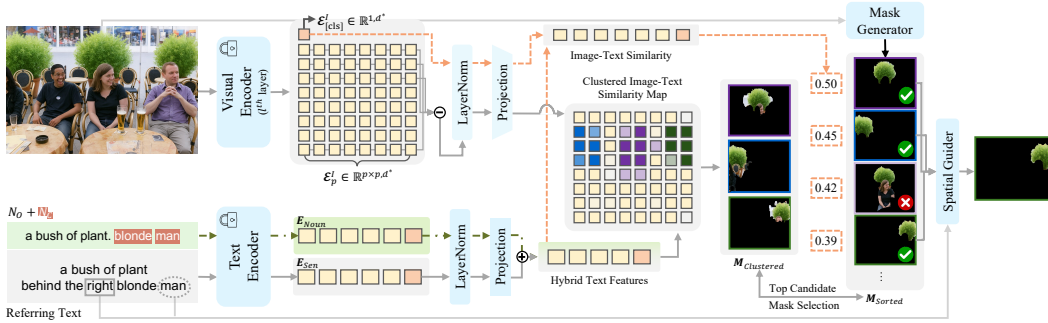


Figure 2: **The overall design of our COPATCH framework.** Our context-aware spatial map, CoMap, (*i.e.*, clustered image-text similarity map) is generated using: 1) Patch-level image features extracted from the l -th layer of the visual encoder. 2) Hybrid text features extracted with the combination of the global sentence and local primary noun and context token features. The spatial map is then used to select better top mask candidates, enabling precise final mask selection.

components: 1) Hybrid text features with *context tokens*, which preserve spatial cues in referring expressions (Section 3.1), and 2) context-aware spatial map, CoMap, generated by our enhanced text and spatial-aware image features (Section 3.2). Unlike prior zero-shot RIS methods that rely on minimal noun-phrase anchors or coarse spatial grounding signals (*e.g.*, GradCAM in Figure 1c), our design utilizes inherently embedded contextual tokens and spatial information from intermediate layers to enable richer spatial grounding at a lower cost.

3.1 CONTEXT TOKEN (CT) EXTRACTION FOR REFINED HYBRID TEXT FEATURES

Motivation. Previous studies have demonstrated the effectiveness of hybrid text features that combine global and local-level features. Herein, the local text feature encodes only the primary noun phrase. Specifically, it is commonly extracted as the primary noun phrase (Yu et al., 2023; Liu & Li, 2025) or chunk (Wang et al., 2025). However, this could leave out important spatial cues that might appear after the selected noun phrase (*e.g.*, “woman smiling” in “a bush of plant behind a middle woman smiling” in Figure 1a). Without appending contextual cues, different expressions may collapse to the same mask, limiting spatial disambiguation. Here, we hypothesize that augmenting context information when generating local-level features could improve spatial grounding.

Method. We construct hybrid text features that fuse both global and context-aware local representations. Given the referring expression t , we first extract global-level text features by feed-forwarding the entire text input into the text encoder (ϕ_T), resulting in $E_{\text{Sen}} (= \phi_T(t))$. For local features, we extract two parts: primary noun phrase (N_O) and the context token (N_C) (implementation details in Appendix B.1). Then, these two chunks are concatenated at an input level and encoded jointly, generating $E_{\text{Noun}} (= \phi_T([N_O|N_C]))$. Lastly, we merge the global-level and local-level text features by addition per hidden dimension ($E_{\text{ConText}} = \gamma E_{\text{Sen}} + (1 - \gamma) E_{\text{Noun}} \in \mathbb{R}^d$). Our final hybrid text feature is then used for generating our context-aware spatial map (similar attention-level merging in Appendix C.8). Unlike previous hybrid feature approaches that restrict local features to a single noun phrase, our formulation guides the model with better spatial cues from the contextual tokens for localizing target objects. This yields a more discriminative textual representation, serving as the foundation for our context-aware spatial map introduced in the next subsection.

3.2 CONTEXT-AWARE SPATIAL MAP FOR TOP CANDIDATE (TC) MASK SELECTION

Motivation. Although CLIP is often described as spatially blind (Tong et al., 2024; Tang et al., 2023; Kamath et al., 2023; Du et al., 2024; Yuksekgonul et al., 2023; Yu et al., 2023), we claim that this perception largely stems from their use of the original image extraction pathway. In CLIP, the final image feature is extracted as a single global vector at its final layer for image-text alignment, rendering the model inherently spatially agnostic. Our analysis reveals that its intermediate layers retain valuable, discriminative spatial information. Figure 3 illustrates that the cosine similarity

between position-shifted images decreases with increasing layer depth, rising steeply at the final layer (unlike image-only feature extractor, DINO (Zhang et al., 2023; Tong et al., 2024)). This observation motivates us to explicitly leverage intermediate patch embeddings, rather than using final-layer image features, for constructing our own spatial map.

Method – Stage 1: Context-Aware Spatial Map Generation. To better capture spatial cues, we compute image–text similarity at the patch level. Given the image v , we extract patch-level image embeddings using the l -th layer of the visual encoder (ϕ_V^l). At the l -th layer, we forward the patch-level image embeddings, $\mathcal{E}_p^l \in \mathbb{R}^{p \times p \times d^*}$ into the post layer norm (LN). These embeddings are normalized and projected into the joint embedding space using the pretrained projection layer, resulting in the following patch-level image features: $E_p^l = \text{LN}(\mathcal{E}_p^l) \cdot \mathbb{W}_{d^* \rightarrow d} \in \mathbb{R}^{p \times p \times d}$.

We then compute the patch-level similarity map as follows: $\tilde{\mathcal{M}}^l = (\tilde{\mathcal{M}}_{ij}^l)_{1 \leq i, j \leq p} \in \mathbb{R}^{p \times p}$, where $\tilde{\mathcal{M}}_{ij}^l = \cos(E_p^l[i, j], E_{\text{ConText}})$, $\forall i, j \in \{1, \dots, p\}$. This map highlights how strongly each image patch aligns with the referring expression, offering a spatially-enhanced alternative to the original CLIP’s image features. Based on a property of cosine similarity, we correct an inversion artifact (see Appendix B.2) previously noted in Li et al. (2023) that appears in $\tilde{\mathcal{M}}^l$. We negate the patch embeddings before normalization as follows: $\mathcal{M}_{ij}^l = \cos(\tilde{E}_p^l[i, j], E_{\text{ConText}}^\top)$, where $\tilde{E}_p^l[i, j] = \text{LN}(-\mathcal{E}_p^l[i, j]) \cdot \mathbb{W}_{d^* \rightarrow d}$. Unlike prior methods that rely solely on CLIP’s global representation, this step directly restores spatial sensitivity from intermediate layers.

Method – Stage 2: Mask Selection via Clustered Context-Aware Spatial Map (CoMap).

We present a framework to select the final mask out of mask candidates (M ’s) generated from pretrained segmentation models, utilizing \mathcal{M}^l . To convert the patch-level activations into coherent spatial cues, we cluster adjacent patches with high similarity (Figure 4). Adjacent patches with high similarity form the same clusters, which are then interpolated into the final context-aware spatial map, CoMap.

The map is used to rerank the top candidate masks (M_{Sorted} in Figure 2) selected based on the original image–text similarity: $\mathcal{S}^m = \cos(E_{\text{Img}}^m, E_{\text{ConText}}^\top) \in \mathbb{R}$, $\forall m = 1, \dots, M$ (M : # of predicted masks per sample). Specifically, we sort candidate masks ($M_{\text{Clustered}}$ in Figure 2) based on their degree of overlap with all generated clusters from CoMap. Then, $M_{\text{Clustered}}$ is used to filter out M_{Sorted} by 1) leaving the first candidate mask from M_{Sorted} and 2) reranking the top- $(k - 1)$ candidate masks from M_{Sorted} based on the overlap with $M_{\text{Clustered}}$. Among these top- k candidate masks, the final mask is selected to be compared with the ground-truth mask (top- k performance is also reported to validate the top- k candidate masks). The selection is based on the similarity between our hybrid

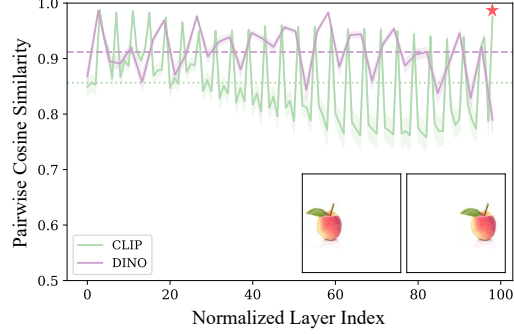


Figure 3: **Cosine similarity trend across layers for image pairs containing objects at different locations.** An overall decreasing trend is observed with a high peak (~ 1.0) at the last layer (indicated by \star) for CLIP.

Algorithm 1 Spatial Map Clustering

```

Require: Spatial map  $\mathcal{M} \in \mathbb{R}^{p \times p}$ 
1:  $\mathcal{B} = (\mathcal{B}_{ij})$ , where  $\forall i, j: \mathcal{B}_{ij} \leftarrow [\mathcal{M}_{ij} > \delta]$ 
2:  $\mathcal{C} \leftarrow \mathbf{0}_{p \times p}$ ,  $l \leftarrow 0$ 
3: for each patch coordinate  $\mathbf{k}$  in  $\mathcal{B}$  do
4:   if  $\mathcal{B}[\mathbf{k}] = 1$  and  $\mathcal{C}[\mathbf{k}] = 0$  then
5:      $l \leftarrow l + 1$ 
6:      $Q \leftarrow \text{new Queue}()$ 
7:      $Q.\text{push}(\mathbf{k})$ ,  $\mathcal{C}[\mathbf{k}] \leftarrow l$ 
8:     while  $Q$  is not empty do
9:        $\mathbf{p} \leftarrow Q.\text{pop}()$ 
10:      for each neighbor  $\mathbf{n}$  of  $\mathbf{p}$  do
11:        if  $\mathbf{n}$  is valid and  $\mathcal{B}[\mathbf{n}] = 1$  and
12:           $\mathcal{C}[\mathbf{n}] = 0$  then
13:             $Q.\text{push}(\mathbf{n})$ ,  $\mathcal{C}[\mathbf{n}] \leftarrow l$ 
14:          end if
15:        end for
16:      end while
17:    end if
18:  end for
19: return Interpolated  $\mathcal{C}$ 

```

Figure 4: **Clustering algorithm for CoMap generation.** Clusters of the spatial map are formed by threshold-exceeding adjacent patches and interpolated into the final spatial map, CoMap (or \mathcal{C}).

	Pretrained Models	RefCOCOg		RefCOCO			RefCOCO+			
		val (U)	test (U)	val (G)	val	testA	testB	val	testA	testB
Zero-shot RIS methods (CLIP ViT-B/32)										
Region Token (Suo et al., 2023; Li et al., 2022a)	-	16.33	16.88	17.31	17.06	18.02	16.28	18.83	20.31	17.78
CLIPSurgery (Li et al., 2023)	-	20.44	21.80	21.23	18.04	14.34	21.28	18.39	14.34	22.98
Cropping (Yu et al., 2023)	FreeSOLO	31.88	30.94	31.06	24.83	22.58	25.72	26.33	24.06	26.46
Global-Local (Yu et al., 2023)	FreeSOLO	33.52	33.67	33.61	26.20	24.94	26.56	27.80	25.64	27.84
Global-Local [†]	FreeSOLO	32.23	33.11	31.80	23.90	21.74	25.85	24.18	21.97	26.45
Global-Local (Yu et al., 2023; Suo et al., 2023)	SAM	42.02	42.02	42.67	32.93	34.93	30.09	38.37	42.05	32.65
HybridGL [†] (Liu & Li, 2025)	SAM	44.52	44.93	44.52	38.26	39.43	37.91	36.04	38.65	32.07
TAS (Suo et al., 2023)	SAM, BLIP-2	46.62	46.80	48.05	39.84	41.08	46.24	43.63	49.13	36.54
COPATCH (Top-1)	Mask2Former	52.24	52.15	51.69	46.76	52.09	40.18	44.07	50.66	35.86
COPATCH (Top-3)	Mask2Former	68.52	68.19	68.73	62.25	66.20	59.51	65.64	69.71	61.40
Mask2Former Upper Bound [†]	-	76.85	77.56	76.85	79.73	81.35	76.49	79.75	81.35	76.57
Zero-shot RIS methods (CLIP ViT-B/16)										
CaR (Sun et al., 2024)	SAM	36.67	36.57	36.63	33.57	35.36	30.51	34.22	36.03	31.02
Ref-Diff (Ni et al., 2023)	SAM, SD	44.02	44.51	44.26	37.21	38.40	37.19	37.29	40.51	33.01
HybridGL (Ni et al., 2023)	SAM	51.25	51.59	-	49.48	53.37	45.19	43.40	49.13	37.17
COPATCH (Top-1)	Mask2Former	54.42	55.62	54.71	50.05	55.38	43.01	46.83	54.08	37.67
COPATCH (Top-3)	Mask2Former	71.21	72.29	72.11	65.38	67.77	62.45	67.41	69.86	63.83
Zero-shot RIS methods (DFN ViT-H/14)										
COPATCH (Top-1)	Mask2Former	56.23	55.88	55.68	50.91	56.59	44.79	47.05	54.12	38.91
COPATCH (Top-3)	Mask2Former	74.23	74.90	75.04	68.33	72.00	65.55	71.26	74.22	68.04
Weakly/Pseudo-supervised RIS methods										
CHUNK (ALBEF) (Lee et al., 2023a)	-	32.90	-	-	31.10	32.30	30.10	31.30	32.10	30.10
TSEG (ViT-S/16 & BERT) (Strudel et al., 2022)	-	23.41	-	-	25.95	-	-	22.62	-	-
PPT (CLIP ViT-B/16) (Dai & Yang, 2024)	SAM	42.97	-	-	46.76	45.33	46.28	45.34	45.84	44.77
Pseudo-RIS (ResNet50) (Yu et al., 2024)	SAM, CoCa	45.99	46.67	46.80	41.05	48.19	33.48	44.33	51.42	35.08

Table 1: **Comparison of mIoU performances across zero-shot and weakly/pseudo-supervised RIS methods on RefCOCOg, RefCOCO, and RefCOCO+ datasets.** We attain the overall best performances for CLIP (ViT-B/32 and ViT-B/16) and DFN (ViT-H/14), outperforming the SoTA, TAS (Suo et al., 2023), and HybridGL (Liu & Li, 2025). [†] stands for the reproduced results.

text features and negative text features (*i.e.*, features of primary noun(s) that come after the positional relation) if there is an explicit spatial cue (*e.g.*, ‘behind’) using the spatial guider (*i.e.*, Spatial Coherence or SC from Liu & Li (2025)).

Our approach challenges the prevailing assumption that CLIP is spatially blind by unlocking latent spatial knowledge from its intermediate representations. In contrast to prior methods that rely on computationally intensive gradient techniques or attention maps, our approach directly extracts spatially-aware features using our CoMap. This training-free extraction without recomputation is not only more efficient but also more faithful to the model’s inherent spatial understanding.

4 EXPERIMENTS

4.1 EXPERIMENTAL SETTINGS

The details on the datasets and evaluation metrics are in Appendix A. For implementation, we use CLIP (ViT-B/32 and ViT-B/16) (Radford et al., 2021) as a model backbone to ensure a fair comparison with previous zero-shot RIS methods, as well as DFN (ViT-H/14) (Fang et al., 2023) that shows a better spatial grounding capability among CLIP variations (Tong et al., 2024). Before the final evaluation, we perform a hyperparameter search to find the optimal exit layer (l) of the visual encoder, the initial threshold (δ), and the proportion of spatial coherence (α) (Section 3.2). This is conducted using only a 10% of the RefCOCOg val set, and we use fixed l , δ , and α for all evaluations (l : 10, 8, and 22, δ : 0.5, 0.3, 0.5, and α : 0.5, 0.7, and 0.5 for COPATCH (CLIP ViT-B/32, CLIP ViT-B/16, and DFN ViT-H/14).

		Train Dataset	All	Unseen
Zero-shot RIS methods				
Global-Local (Yu et al., 2023)	✗	23.64	22.98	
Global-Local [†]	✗	22.43	21.54	
TAS (Suo et al., 2023)	✗	25.64	24.66	
Ref-Diff (Ni et al., 2023)	✗	29.42	-	
IterPRIM-E (Wang et al., 2025)	✗	38.10	37.90	
HybridGL (Liu & Li, 2025)	✗	38.39	-	
HybridGL [†]	✗	37.60	37.91	
COPATCH (Top-1)	✗	38.53	38.31	
COPATCH (Top-3)	✗	45.36	45.14	
Supervised RIS methods				
CRIS (Wang et al., 2022b)	RefCOCO	15.53	13.75	
	RefCOCO+	16.30	14.62	
	RefCOCOg	16.24	13.88	
	RefCOCO	16.68	14.43	
LAVT (Yang et al., 2022)	RefCOCO+	16.64	13.49	
	RefCOCOg	16.05	13.48	
	RefCOCO+	28.68	29.14	
Pseudo-RIS (Yu et al., 2024)	PhraseCut	32.75	33.52	

Table 2: **Comparison of oIoU performances across zero-shot and supervised RIS methods on PhraseCut dataset.** COPATCH (CLIP ViT-B/16) surpasses all the existing methods, including Pseudo-RIS (Yu et al., 2024) trained on PhraseCut datasets.

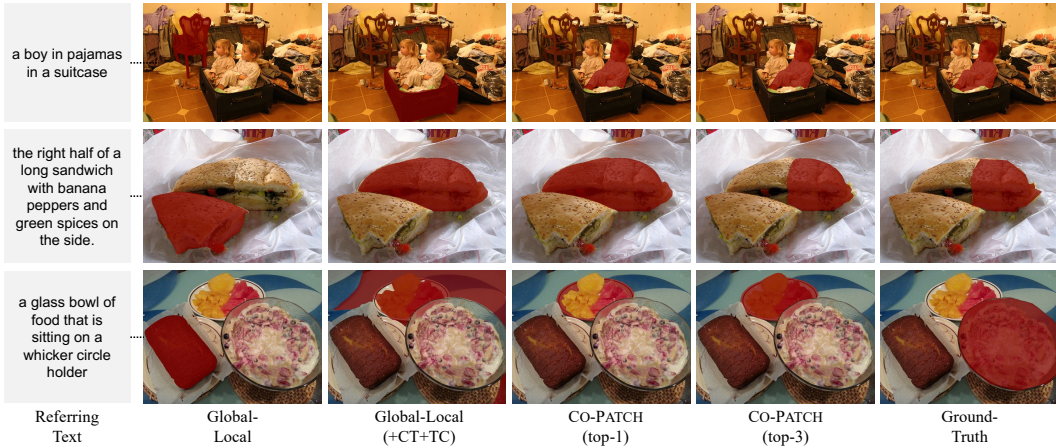


Figure 5: **Qualitative comparison across zero-shot RIS methods.** Our CoPATCH demonstrates strong spatial grounding ability. The first row shows a case where both CoPATCH top-1 and top-3 methods segment correctly compared to Global-Local (Yu et al., 2023) and new Global-Local (+CT+TC, as in Table 3a). The second row captures a case that is incorrectly segmented using CoPATCH (top-1) but accurately segmented on the “right half” with CoPATCH (top-3).

4.2 MAIN RESULTS

Comparison to State of the Arts. As shown in Table 1 (more performance results in Appendices C.3 and C.10) and Figure 5, we achieve notable superior performance over existing SoTA zero-shot methods (Yu et al., 2023; Suo et al., 2023; Liu & Li, 2025; Ni et al., 2023; Li et al., 2023; Sun et al., 2024), even higher than the results of weakly- and pseudo-supervised approaches (Strudel et al., 2022; Lee et al., 2023a; Yu et al., 2024) (the results using different pretrained models in Appendix C.2). In particular, our CoPATCH (DFN ViT-H/14) attains the best results on 8 out of 9 evaluation splits. CoPATCH with CLIP backbones also demonstrates strong performance and is enhanced further if the final mask is selected among the top-3 candidate masks generated using our CoMap. For example, in the RefCOCOg validation (U) and test sets with ViT-B/32, we observe gains of +16.28 and +16.04 mIoU, respectively. These results reach 89.16% and 87.91% of the mask upper bound (oracle) performances, indicating that the top candidate masks selected using the clusters from CoMap are highly informative in locating the target object (Figure 5, second row). Although there are still several cases where CoPATCH may not be able to segment correctly due to CLIP’s limited understanding of some vocabularies (e.g., “glass” in Figure 5, third row), our approach achieves the best results even on the very challenging PhraseCut dataset. We obtain oIoU scores of 38.41 (*all*) and 38.12 (*unseen*), outperforming recent SoTA zero-shot and supervised methods (Table 2). These results highlight the robustness and generalizability of our method across various datasets.

Spatial Subset Evaluation. To evaluate the fine-grained spatial grounding ability of CLIP, we conduct a targeted evaluation on samples that contain explicit spatial cues (e.g., “left”, “bottom”, and “closest to”). To identify such samples, we utilize Qwen2.5-14B-Instruct (Yang et al., 2024) to classify each referring expression as spatial or non-spatial and extract the cue if present (prompt details in Appendix C.6). These automatically generated annotations take up 50.72%, 62.40%, and 23.48% of the validation samples in RefCOCOg, RefCOCO, and RefCOCO+. Figure 6 shows significant gains using CoPATCH over the baseline, with +20.83% and +15.55% mIoU im-

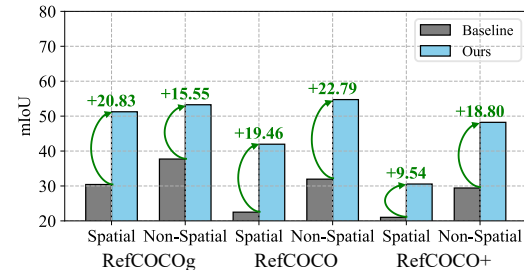


Figure 6: **Subset performance comparison between Global-Local (Yu et al., 2023) and Co-PATCH.** We observe a significant gain for all the spatial and non-spatial validation subsets.

provements on the spatial and non-spatial subsets of RefCOCOg. These improvements demonstrate that our spatial map **CoMap** contributes to the gains on spatial subsets, while the integration of context-aware tokens enhances performance on non-spatial subsets by providing richer semantic information.

4.3 ABLATION STUDIES AND ANALYSIS

Spatial Map Analysis. We analyze the effectiveness of our **CoMap** by comparing it with the widely-used Grad-CAM (Selvaraju et al., 2016) used in SoTA zero-shot RIS method with ALBEF (Li et al., 2021) as backbone, IteR-PrimE (Wang et al., 2025). Figure 7 illustrates a qualitative comparison between Grad-CAM (used in IteRPrimE) and **CoMap** used in our method. We observe that **CoMap** better captures target objects in many cases (e.g., “chair” in the first column). Moreover, **CoMap** (ViT-B/16) achieves better average performance (e.g., +6.9 mIoU) with lower inference latency (e.g., -2.95 sec. per sample), as shown in the Appendix C.1.

In addition, we evaluate how our spatial map contributes to the quality of top candidate masks. Unlike prior methods (Yu et al., 2023) that rely on global image-text cosine similarity, our map captures fine-grained patch-level spatial correspondences. This is particularly important in scenarios where distinguishing targets according to their spatial configuration is essential for accurate localization. To reflect this challenge, we design our experiments to select the final mask given different numbers of top candidate masks. Table 3a shows that our approach consistently outperforms Global-Local, demonstrating the effectiveness of our **CoMap** for generating accurate and reliable region proposals (qualitative results in Figure 8). Specifically, we select top- k candidate masks based on the ranking of original image-text similarity for Global-Local and new image-text similarity reranked using the automatically generated clusters from **CoMap** for COPATCH. Using the top three candidate masks consistently yields the best performance (Table 3a) and sufficient diversity (Figure 8) for the final mask selection.

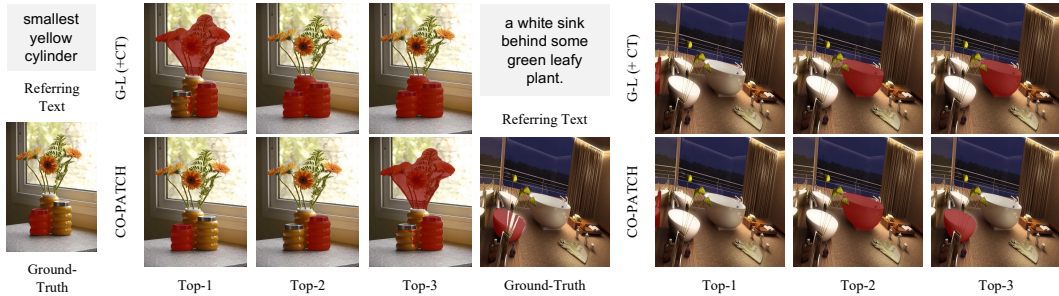


Figure 8: **Qualitative comparison of top candidate masks generated using original image-text similarity from Global-Local (w/ CT) and averaged CoMap similarity score using our COPATCH.** The top candidate masks generated using our method show better diversity and accuracy.

Subcomponents. Table 3b demonstrates the effectiveness of the core components of COPATCH – Context Token (CT) extraction (Section 3.1) and Top Candidate (TC) mask selection (Section 3.2). We use Global-Local (Yu et al., 2023) as the backbone image/text extraction method since the vanilla performances are higher than those of HybridGL (Liu & Li, 2025) (e.g., 5.53 higher mIoU on ViT-B/32). We find that using our CT alone helps the models to achieve higher performances, especially in ViT-B/32 (e.g.+2.58 for mIoU; qualitative results in Appendix C.5). After the text feature extraction, mask scoring with top candidate masks from our ranked clusters (*i.e.*, TC) proves more

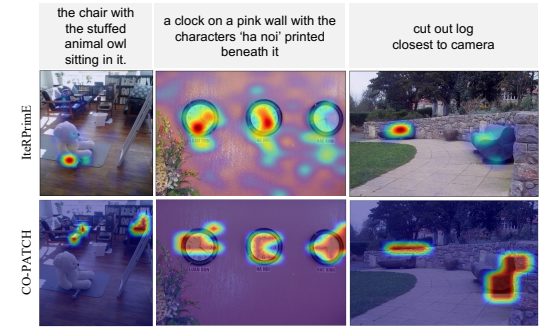


Figure 7: **Spatial map comparison of Grad-CAM used in IteRPrimE and CoMap used in our COPATCH.** Our spatial map better localizes the target objects (e.g., “chair”, “clock”, “log”) in referring expressions.

Top Candidate Mask Number	Global-Local		COPATCH	
	mIoU	oIoU	mIoU	oIoU
2	50.47	40.28	52.08	40.72
3	50.79	41.29	52.24	41.43
4	49.42	40.81	51.92	41.40
k	—	—	51.80	41.43

(a) **Comparison of zero-shot RIS performances using top candidates selected by the original and our candidate mask scores on RefCOCOg val (U) set.**

	CT	TC	SC	ViT-B/32		ViT-B/16	
				mIoU	oIoU	mIoU	oIoU
HybridGL				41.54	29.89	46.59	37.04
CoPATCH	✓			42.58	30.77	47.01	37.36
Global-Local				47.07	35.73	50.30	38.35
CoPATCH	✓			49.65	37.18	50.65	38.24
Global-Local	✓	✓		47.70	36.32	50.68	38.84
CoPATCH	✓	✓		50.16	37.63	51.16	38.84
Global-Local	✓	✓	✓	50.42	38.17	50.91	39.58
CoPATCH	✓	✓	✓	52.24	41.43	54.42	44.14

(b) **Comparison of zero-shot RIS performances without and with each subcomponent.**

Table 3: **Ablation study results using different numbers of top mask candidates and subcomponents.** (a) Our performances are consistently greater than when using top mask candidates selected by Global-Local (Yu et al., 2023) (k : # of automatically generated clusters that differ per data sample). (b) Using the baseline feature extraction methods—Global-Local (Yu et al., 2023) and HybridGL (Liu & Li, 2025), all the subcomponents, Context Token (CT), Top Candidate (TC), and Spatial Coherence (SC) are integral for building COPATCH.

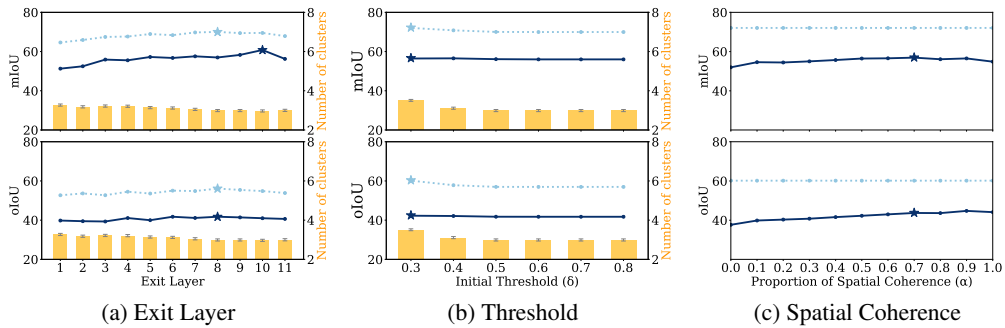


Figure 9: **Hyperparameter tuning results for COPATCH (ViT-B/16) using 10% of the RefCOCOg val set.** The **deep-blue** and **sky-blue** lines depict **top-1** and **top-3** performances across exit layers. The **golden** bars represent the number of clusters averaged across data instances for each exit layer. The overall IoU performance is insensitive to a particular hyperparameter value.

effective than the previous approach (Liu & Li, 2025), which ranks masks solely by the cosine similarity between raw image and text features. Specifically, our method achieves improvements of +2.46 and +1.32 mIoU and oIoU on ViT-B/32. Finally, the mIoU and oIoU performances improve by 2.80% and 4.18% using Spatial Coherence (SC) (Liu & Li, 2025). These results confirm that each component of COPATCH contributes meaningfully, and their synergy is crucial for achieving strong zero-shot RIS performance.

Hyperparameters. Figure 9 shows the performance change across different exit layers (Appendix C.9), initial threshold, and proportion of the spatial coherence method (Liu & Li, 2025). We observe no significant drop in performance across varying hyperparameters tuned on 10% of the RefCOCOg validation set (Mao et al., 2016). For all experiments in the main paper (Tables 1 and 2), we use a single fixed hyperparameter configuration (Appendix C.7). Despite this global setting, COPATCH consistently outperforms previous methods across benchmarks, demonstrating that our method is robust and generalizes well without requiring dataset-specific tuning. However, more optimal performances could also be achieved if hyperparameter tuning is performed.

5 CONCLUSION

We propose COPATCH, a novel zero-shot RIS framework that addresses the spatial limitations of CLIP by improving both its text and image representations. On the text side, COPATCH enriches linguistic understanding by incorporating spatially informative context tokens, including beyond primary noun phrases commonly used in prior works. On the image side, we exploit spatial information

preserved in CLIP’s intermediate layers to generate fine-grained patch-level image features. These are used to compute the context-aware spatial map, CoMap , which enables accurate top mask selection. Experimental results demonstrate that COPATCH consistently outperforms the SoTA zero-shot RIS methods across RefCOCO, RefCOCO+, RefCOCOg, and PhraseCut benchmarks, with 2–7% gains across different CLIP architectures. Notably, we achieve a 10–21% improvement on a challenging spatial subset. Our synergistic approach to enhancing both visual and textual representations opens promising directions for spatially-grounded, semantically-robust zero-shot segmentation.

REFERENCES

Na Min An, Hyeonhee Roh, Sein Kim, Jae Hun Kim, and Maesoon Im. Reinforcement learning framework to simulate short-term learning effects of human psychophysical experiments assessing the quality of artificial vision. In *2023 International Joint Conference on Neural Networks (IJCNN)*, pp. 1–8. IEEE, 2023.

Na Min An, Sania Waheed, and James Thorne. Capturing the relationship between sentence triplets for LLM and human-generated texts to enhance sentence embeddings. In Yvette Graham and Matthew Purver (eds.), *Findings of the Association for Computational Linguistics: EACL 2024*, pp. 624–638, St. Julian’s, Malta, March 2024. Association for Computational Linguistics. URL <https://aclanthology.org/2024.findings-eacl.43/>.

Na Min An, Eunki Kim, James Thorne, and Hyunjung Shim. IOT: Embedding standardization method towards zero modality gap. In Wanxiang Che, Joyce Nabende, Ekaterina Shutova, and Mohammad Taher Pilehvar (eds.), *Proceedings of the 63rd Annual Meeting of the Association for Computational Linguistics (Volume 1: Long Papers)*, pp. 27182–27199, Vienna, Austria, July 2025a. Association for Computational Linguistics. ISBN 979-8-89176-251-0. doi: 10.18653/v1/2025.acl-long.1319. URL <https://aclanthology.org/2025.acl-long.1319/>.

Na Min An, Hyeonhee Roh, Sein Kim, Jae Hun Kim, and Maesoon Im. Machine learning techniques for simulating human psychophysical testing of low-resolution phosphene face images in artificial vision. *Advanced Science*, 12(15):2405789, 2025b.

Sule Bai, Yong Liu, Yifei Han, Haoji Zhang, and Yansong Tang. Self-calibrated clip for training-free open-vocabulary segmentation. *arXiv preprint arXiv:2411.15869*, 2024.

Aude Billard and Danica Kragic. Trends and challenges in robot manipulation. *Science*, 364(6446):eaat8414, 2019.

Walid Bousselham, Felix Petersen, Vittorio Ferrari, and Hilde Kuehne. Grounding everything: Emerging localization properties in vision-language transformers. In *Proceedings of the IEEE/CVF Conference on Computer Vision and Pattern Recognition*, pp. 3828–3837, 2024.

Agneet Chatterjee, Yiran Luo, Tejas Gokhale, Yezhou Yang, and Chitta Baral. Revision: Rendering tools enable spatial fidelity in vision-language models. In *European Conference on Computer Vision*, pp. 339–357. Springer, 2024.

Li Chen, Penghao Wu, Kashyap Chitta, Bernhard Jaeger, Andreas Geiger, and Hongyang Li. End-to-end autonomous driving: Challenges and frontiers. *IEEE Transactions on Pattern Analysis and Machine Intelligence*, 2024.

Bowen Cheng, Ishan Misra, Alexander G Schwing, Alexander Kirillov, and Rohit Girdhar. Masked-attention mask transformer for universal image segmentation. In *Proceedings of the IEEE/CVF conference on computer vision and pattern recognition*, pp. 1290–1299, 2022.

Qiyuan Dai and Sibei Yang. Curriculum point prompting for weakly-supervised referring image segmentation. In *Proceedings of the IEEE/CVF Conference on Computer Vision and Pattern Recognition*, pp. 13711–13722, 2024.

Mengfei Du, Biniao Wu, Zejun Li, Xuanjing Huang, and Zhongyu Wei. Emb spatial-bench: Benchmarking spatial understanding for embodied tasks with large vision-language models, 2024. URL <https://arxiv.org/abs/2406.05756>.

Alex Fang, Albin Madappally Jose, Amit Jain, Ludwig Schmidt, Alexander Toshev, and Vaishaal Shankar. Data filtering networks. *arXiv preprint arXiv:2309.17425*, 2023.

Zeyu Han, Fangrui Zhu, Qianru Lao, and Huaizu Jiang. Zero-shot referring expression comprehension via structural similarity between images and captions. In *Proceedings of the IEEE/CVF Conference on Computer Vision and Pattern Recognition*, pp. 14364–14374, 2024.

Matthew Honnibal. spacy 2: Natural language understanding with bloom embeddings, convolutional neural networks and incremental parsing. (*No Title*), 2017.

Kaiyi Huang, Kaiyue Sun, Enze Xie, Zhenguo Li, and Xihui Liu. T2i-compbench: A comprehensive benchmark for open-world compositional text-to-image generation. *Advances in Neural Information Processing Systems*, 36:78723–78747, 2023.

Han-Young Jang, Hadi Moradi, Suyeon Hong, Sukhan Lee, and JungHyun Han. Spatial reasoning for real-time robotic manipulation. In *2006 IEEE/RSJ International Conference on Intelligent Robots and Systems*, pp. 2632–2637. IEEE, 2006.

Amita Kamath, Jack Hessel, and Kai-Wei Chang. What’s “up” with vision-language models? investigating their struggle with spatial reasoning, 2023. URL <https://arxiv.org/abs/2310.19785>.

Dongseob Kim, Seungho Lee, Junsuk Choe, and Hyunjung Shim. Weakly supervised semantic segmentation for driving scenes. In *Proceedings of the AAAI conference on artificial intelligence*, volume 38, pp. 2741–2749, 2024.

Dongwon Kim, Namyup Kim, Cuiling Lan, and Suha Kwak. Shatter and gather: Learning referring image segmentation with text supervision. In *Proceedings of the IEEE/CVF International Conference on Computer Vision*, pp. 15547–15557, 2023a.

Seoyeon Kim, Minguk Kang, Dongwon Kim, Jaesik Park, and Suha Kwak. Extending clip’s image-text alignment to referring image segmentation. *arXiv preprint arXiv:2306.08498*, 2023b.

Alexander Kirillov, Eric Mintun, Nikhila Ravi, Hanzi Mao, Chloe Rolland, Laura Gustafson, Tete Xiao, Spencer Whitehead, Alexander C Berg, Wan-Yen Lo, et al. Segment anything. In *Proceedings of the IEEE/CVF international conference on computer vision*, pp. 4015–4026, 2023.

Jungbeom Lee, Sungjin Lee, Jinseok Nam, Seunghak Yu, Jaeyoung Do, and Tara Taghavi. Weakly supervised referring image segmentation with intra-chunk and inter-chunk consistency. In *Proceedings of the IEEE/CVF International Conference on Computer Vision*, pp. 21870–21881, 2023a.

Noah Lee, Na Min An, and James Thorne. Can large language models capture dissenting human voices? In *Proceedings of the 2023 Conference on Empirical Methods in Natural Language Processing*, pp. 4569–4585, 2023b.

Jiahao Li, Greg Shakhnarovich, and Raymond A Yeh. Adapting clip for phrase localization without further training. *arXiv preprint arXiv:2204.03647*, 2022a.

Junnan Li, Ramprasaath Selvaraju, Akhilesh Gotmare, Shafiq Joty, Caiming Xiong, and Steven Chu Hong Hoi. Align before fuse: Vision and language representation learning with momentum distillation. *Advances in neural information processing systems*, 34:9694–9705, 2021.

Junnan Li, Dongxu Li, Caiming Xiong, and Steven Hoi. Blip: Bootstrapping language-image pre-training for unified vision-language understanding and generation. In *International conference on machine learning*, pp. 12888–12900. PMLR, 2022b.

Yi Li, Hualiang Wang, Yiqun Duan, and Xiaomeng Li. Clip surgery for better explainability with enhancement in open-vocabulary tasks. *arXiv e-prints*, pp. arXiv–2304, 2023.

Feng Liang, Bichen Wu, Xiaoliang Dai, Kunpeng Li, Yinan Zhao, Hang Zhang, Peizhao Zhang, Peter Vajda, and Diana Marculescu. Open-vocabulary semantic segmentation with mask-adapted clip. In *Proceedings of the IEEE/CVF conference on computer vision and pattern recognition*, pp. 7061–7070, 2023.

Fangjian Lin, Jianlong Yuan, Sitong Wu, Fan Wang, and Zhibin Wang. Uninext: Exploring a unified architecture for vision recognition. In *Proceedings of the 31st ACM International Conference on Multimedia*, pp. 3200–3208, 2023.

Tsung-Yi Lin, Michael Maire, Serge Belongie, James Hays, Pietro Perona, Deva Ramanan, Piotr Dollár, and C Lawrence Zitnick. Microsoft coco: Common objects in context. In *Computer vision–ECCV 2014: 13th European conference, zurich, Switzerland, September 6–12, 2014, proceedings, part v 13*, pp. 740–755. Springer, 2014.

Fang Liu, Yuhao Liu, Yuqiu Kong, Ke Xu, Lihe Zhang, Baocai Yin, Gerhard Hancke, and Rynson Lau. Referring image segmentation using text supervision. In *Proceedings of the IEEE/CVF International Conference on Computer Vision*, pp. 22124–22134, 2023.

Ting Liu and Siyuan Li. Hybrid global-local representation with augmented spatial guidance for zero-shot referring image segmentation. *arXiv preprint arXiv:2504.00356*, 2025.

Timo Lüddecke and Alexander Ecker. Image segmentation using text and image prompts. In *Proceedings of the IEEE/CVF conference on computer vision and pattern recognition*, pp. 7086–7096, 2022.

Junhua Mao, Jonathan Huang, Alexander Toshev, Oana Camburu, Alan L Yuille, and Kevin Murphy. Generation and comprehension of unambiguous object descriptions. In *Proceedings of the IEEE conference on computer vision and pattern recognition*, pp. 11–20, 2016.

Varun K Nagaraja, Vlad I Morariu, and Larry S Davis. Modeling context between objects for referring expression understanding. In *Computer Vision–ECCV 2016: 14th European Conference, Amsterdam, The Netherlands, October 11–14, 2016, Proceedings, Part IV 14*, pp. 792–807. Springer, 2016.

Nora Newcombe and Janellen Huttenlocher. *Making space: The development of spatial representation and reasoning*. MIT Press, 2000.

Minheng Ni, Yabo Zhang, Kailai Feng, Xiaoming Li, Yiwen Guo, and Wangmeng Zuo. Ref-diff: Zero-shot referring image segmentation with generative models. *arXiv preprint arXiv:2308.16777*, 2023.

Wujian Peng, Sicheng Xie, Zuyao You, Shiyi Lan, and Zuxuan Wu. Synthesize diagnose and optimize: Towards fine-grained vision-language understanding. In *CVPR*, 2024.

John Piaget. The origins of intelligence in children. *International University*, 1952.

Peng Qi, Yuhao Zhang, Yuhui Zhang, Jason Bolton, and Christopher D Manning. Stanza: A python natural language processing toolkit for many human languages. In *Proceedings of the 58th Annual Meeting of the Association for Computational Linguistics: System Demonstrations*. Association for Computational Linguistics, 2020.

Alec Radford, Jong Wook Kim, Chris Hallacy, Aditya Ramesh, Gabriel Goh, Sandhini Agarwal, Girish Sastry, Amanda Askell, Pamela Mishkin, Jack Clark, et al. Learning transferable visual models from natural language supervision. In *International conference on machine learning*, pp. 8748–8763. PMLR, 2021.

Ramprasaath R Selvaraju, Abhishek Das, Ramakrishna Vedantam, Michael Cogswell, Devi Parikh, and Dhruv Batra. Grad-cam: Why did you say that? *arXiv preprint arXiv:1611.07450*, 2016.

Chao Shang, Zichen Song, Heqian Qiu, Lanxiao Wang, Fanman Meng, and Hongliang Li. Prompt-driven referring image segmentation with instance contrasting. In *Proceedings of the IEEE/CVF Conference on Computer Vision and Pattern Recognition*, pp. 4124–4134, 2024.

Tong Shao, Zhuotao Tian, Hang Zhao, and Jingyong Su. Explore the potential of clip for training-free open vocabulary semantic segmentation. In *European Conference on Computer Vision*, pp. 139–156. Springer, 2024.

Robin Strudel, Ivan Laptev, and Cordelia Schmid. Weakly-supervised segmentation of referring expressions. *arXiv preprint arXiv:2205.04725*, 2022.

Sanjay Subramanian, William Merrill, Trevor Darrell, Matt Gardner, Sameer Singh, and Anna Rohrbach. Reclip: A strong zero-shot baseline for referring expression comprehension. *arXiv preprint arXiv:2204.05991*, 2022.

Shuyang Sun, Runjia Li, Philip Torr, Xiuye Gu, and Siyang Li. Clip as rn: Segment countless visual concepts without training endeavor. In *Proceedings of the IEEE/CVF Conference on Computer Vision and Pattern Recognition*, pp. 13171–13182, 2024.

Yucheng Suo, Linchao Zhu, and Yi Yang. Text augmented spatial aware zero-shot referring image segmentation. In Houda Bouamor, Juan Pino, and Kalika Bali (eds.), *Findings of the Association for Computational Linguistics: EMNLP 2023*, pp. 1032–1043, Singapore, December 2023. Association for Computational Linguistics. doi: 10.18653/v1/2023.findings-emnlp.73. URL <https://aclanthology.org/2023.findings-emnlp.73/>.

Yingtian Tang, Yutaro Yamada, Yoyo Zhang, and Ilker Yildirim. When are lemons purple? the concept association bias of vision-language models. In Houda Bouamor, Juan Pino, and Kalika Bali (eds.), *Proceedings of the 2023 Conference on Empirical Methods in Natural Language Processing*, pp. 14333–14348, Singapore, December 2023. Association for Computational Linguistics. doi: 10.18653/v1/2023.emnlp-main.886. URL <https://aclanthology.org/2023.emnlp-main.886>.

Shengbang Tong, Zhuang Liu, Yuexiang Zhai, Yi Ma, Yann LeCun, and Saining Xie. Eyes wide shut? exploring the visual shortcomings of multimodal llms. In *Proceedings of the IEEE/CVF Conference on Computer Vision and Pattern Recognition*, pp. 9568–9578, 2024.

Xinlong Wang, Zhiding Yu, Shalini De Mello, Jan Kautz, Anima Anandkumar, Chunhua Shen, and Jose M Alvarez. Freesolo: Learning to segment objects without annotations. In *Proceedings of the IEEE/CVF conference on computer vision and pattern recognition*, pp. 14176–14186, 2022a.

Yuji Wang, Jingchen Ni, Yong Liu, Chun Yuan, and Yansong Tang. Iterprime: Zero-shot referring image segmentation with iterative grad-cam refinement and primary word emphasis. In *Proceedings of the AAAI Conference on Artificial Intelligence*, volume 39, pp. 8159–8168, 2025.

Zhaoqing Wang, Yu Lu, Qiang Li, Xunqiang Tao, Yandong Guo, Mingming Gong, and Tongliang Liu. Cris: Clip-driven referring image segmentation. In *Proceedings of the IEEE/CVF conference on computer vision and pattern recognition*, pp. 11686–11695, 2022b.

Thomas Wolbers and Mary Hegarty. What determines our navigational abilities? *Trends in cognitive sciences*, 14(3):138–146, 2010.

Chenyun Wu, Zhe Lin, Scott Cohen, Trung Bui, and Subhransu Maji. Phrasicut: Language-based image segmentation in the wild. In *Proceedings of the IEEE/CVF Conference on Computer Vision and Pattern Recognition*, pp. 10216–10225, 2020.

Zunnan Xu, Zhihong Chen, Yong Zhang, Yibing Song, Xiang Wan, and Guanbin Li. Bridging vision and language encoders: Parameter-efficient tuning for referring image segmentation. In *Proceedings of the IEEE/CVF international conference on computer vision*, pp. 17503–17512, 2023.

An Yang, Baosong Yang, Beichen Zhang, Binyuan Hui, Bo Zheng, Bowen Yu, Chengyuan Li, Dayiheng Liu, Fei Huang, Haoran Wei, et al. Qwen2. 5 technical report. *arXiv preprint arXiv:2412.15115*, 2024.

Zhao Yang, Jiaqi Wang, Yansong Tang, Kai Chen, Hengshuang Zhao, and Philip HS Torr. Lavt: Language-aware vision transformer for referring image segmentation. In *Proceedings of the IEEE/CVF conference on computer vision and pattern recognition*, pp. 18155–18165, 2022.

Seonghoon Yu, Paul Hongsuck Seo, and Jeany Son. Zero-shot referring image segmentation with global-local context features. In *Proceedings of the IEEE/CVF conference on computer vision and pattern recognition*, pp. 19456–19465, 2023.

Seonghoon Yu, Paul Hongsuck Seo, and Jeany Son. Pseudo-ris: Distinctive pseudo-supervision generation for referring image segmentation. In *European Conference on Computer Vision*, pp. 18–36. Springer, 2024.

Mert Yuksekogul, Federico Bianchi, Pratyusha Kalluri, Dan Jurafsky, and James Zou. When and why vision-language models behave like bags-of-words, and what to do about it? In *The Eleventh International Conference on Learning Representations*, 2023. URL <https://openreview.net/forum?id=KRLUvxh8uaX>.

Hao Zhang, Feng Li, Shilong Liu, Lei Zhang, Hang Su, Jun Zhu, Lionel Ni, and Heung-Yeung Shum. Dino: Detr with improved denoising anchor boxes for end-to-end object detection. In *The Eleventh International Conference on Learning Representations*, 2023.

APPENDIX

- Section A: Experimental Setups
- Section B: Method Details
- Section C: Additional Results
- Section D: Discussion

A EXPERIMENTAL SETUPS

Datasets. We evaluate our method on widely used RIS benchmarks: RefCOCO (Nagaraja et al., 2016), RefCOCO+ (Nagaraja et al., 2016), and RefCOCOg (Mao et al., 2016). These datasets have diverse linguistic and visual structures, where RefCOCO and RefCOCO+ have various objects of the same category per image, and RefCOCOg has relatively longer, complex referring expressions (Yang et al., 2022). RefCOCO includes more explicit positional relations (e.g., “left”, “bottom”) than RefCOCO+ and RefCOCOg. In addition, following previous works, we include evaluations on the PhraseCut dataset (Wu et al., 2020), which contains various phrase types such as attributes (e.g., large), categories (e.g., cake), and relationships (e.g., on plate). PhraseCut is evaluated in two settings – *all* (samples) and *unseen*, where the latter indicates evaluation only on samples that do not contain a word from pre-defined 91 MS COCO (Lin et al., 2014) classes.

Evaluation Metrics. For evaluation metrics, we use Mean Intersection over Union (mIoU) and Overall Intersection over Union (oIoU), following related works. The mIoU is computed as the average IoU ($= \frac{|P \cap G|}{|P \cup G|}$, where P : predicted mask generated with a mask generator and G : ground-truth mask) across all data instances. The oIoU is computed as the total intersection over the total union across all samples.

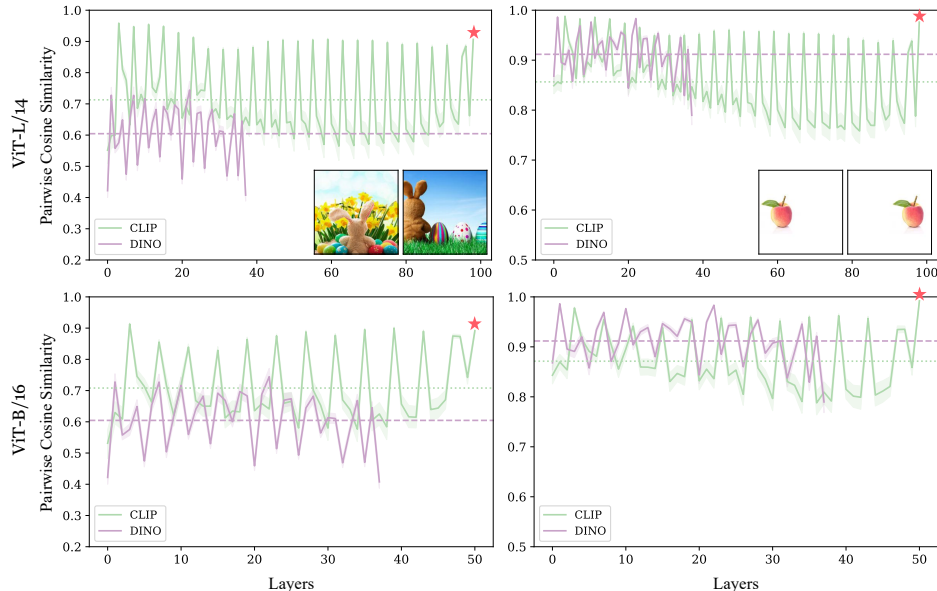


Figure 10: **Varying cosine similarity across layers for image pairs containing objects in different locations for different backbones and datasets.** We observe a decreasing overall trend of similarity for CLIP and a high peak at the last layer.

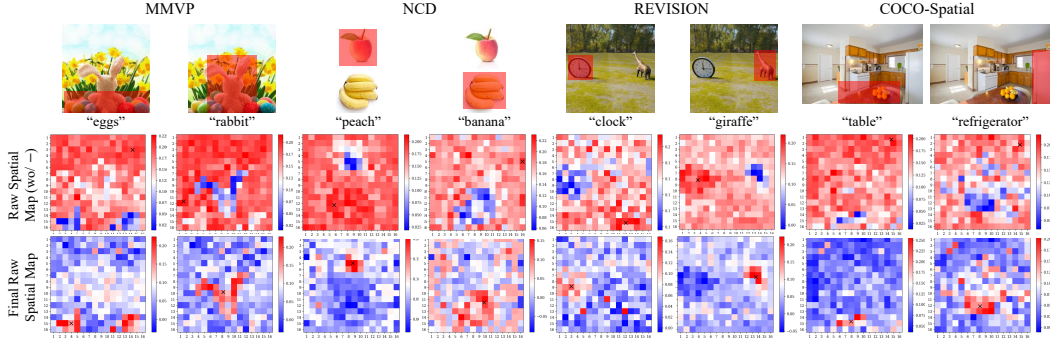


Figure 11: **Opposite visualization without the negation (above) and our final raw spatial map (bottom).** The final raw spatial map localizes the “target objects” and resolves the opposite visualization issue.

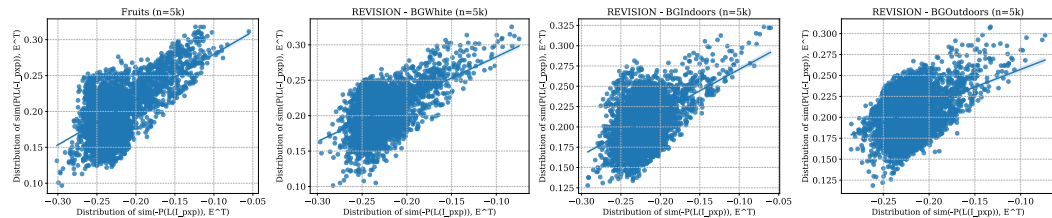


Figure 12: **Correlation plots between our final spatial map (CoMap) image-text similarity scores (y-axis) and negative of the image-text similarity scores from the oppositely visualized spatial map (x-axis).** There exists a strong positive correlation between these two similarity score values across data samples and datasets.

B METHOD DETAILS

B.1 CONTEXT TOKEN (CT) EXTRACTION FOR REFINED HYBRID TEXT FEATURES

Following previous work (Wang et al., 2025), we use the NLP software library, stanza (Qi et al., 2020), to automatically extract N_O and N_C , where N_C are noun or adjective tokens that are not contained in N_O that may appear right side of the primary noun phrase/chunk. Note that we observe a slight performance improvement using stanza instead of spacy (Honnibal, 2017). For instance, using Stanza and Spacy on our method (CoPatch) in the RefCOCOg (val) dataset results in IoU performances of 52.24 and 51.50, respectively. Based on our preliminary analysis, we notice that this method is particularly beneficial when N_C consists of noun chunks that are well-captured by the model (e.g., “woman smiling”) and color adjectives (qualitative results in Appendix C.4).

B.2 NOVEL SPATIAL MAP FOR TOP CANDIDATE (TC) MASK SELECTION

Method – Stage 1: Context-Aware Spatial Map Generation. We explain why the negation operation is necessary to create an intuitive spatial map (CoMap) that resolves the opposite visualization problem described in previous work (Li et al., 2023). To begin with, the spatial map is built based on the observation that the cosine similarity between embeddings of image pairs containing identical objects in different locations is lower in intermediate layers than that of the final layer (Figure 10). This decreasing trend phenomenon implies that the intermediate image embeddings may better preserve spatial information than the original image features extracted from the last layer of the visual encoder.

However, when we calculate the similarity between the hybrid text feature ($E_{\text{ConText}} \in \mathbb{R}^d$) and patch-level image features extracted from the l -th exit layer ($E_p^l \in \mathbb{R}^{p \times p \times d}$), the similarity score values of the resulting similarity map ($\tilde{\mathcal{M}}^l \in \mathbb{R}^{p \times p}$) is shown with opposite visualization (Figure 11). If we simply negate the similarity map itself, the opposite visualization phenomenon is naturally resolved,

but the range of similarity scores falls within -0.3 to 0.0 (x -axis in Figure 12). We could shift these scores by an addition in order to make them fall into the original range of similarity scores (0.0 to 0.3). However, this postprocessing method requires an additional hyperparameter for the shifting and does not fundamentally solve the opposite visualization problem.

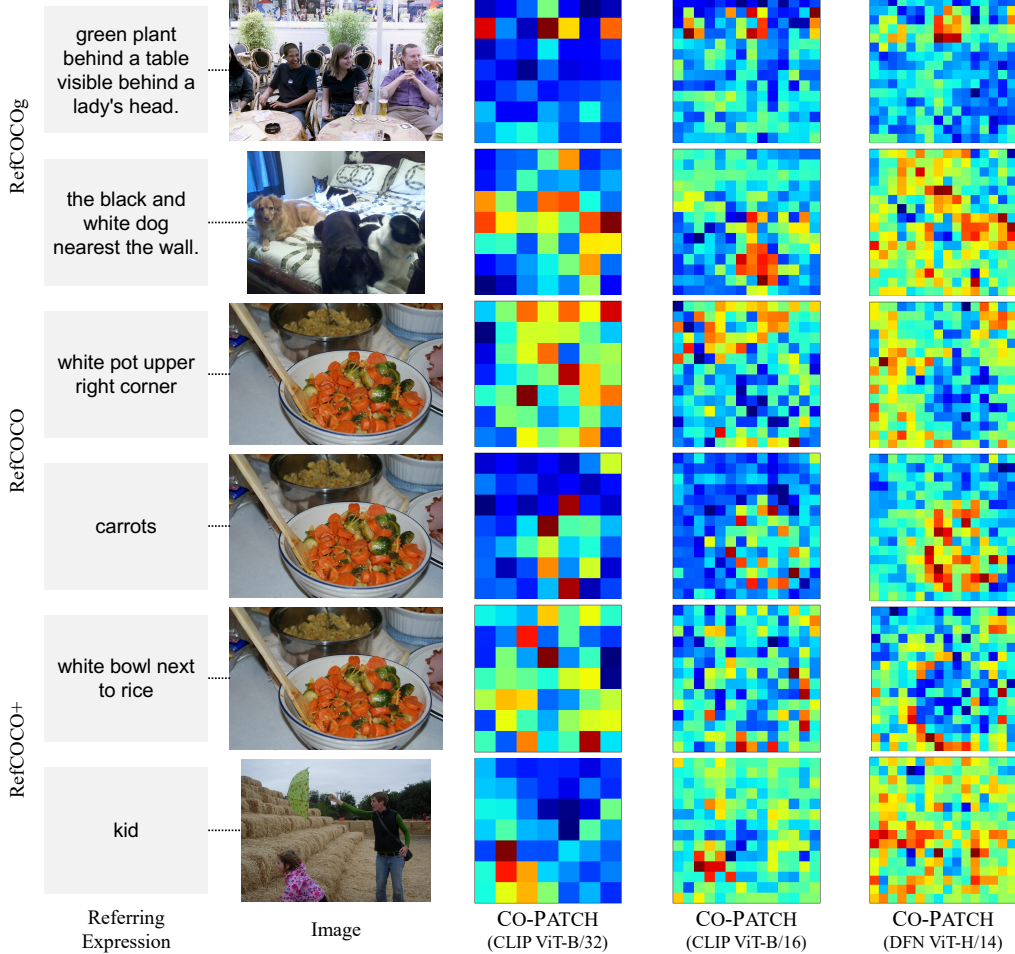


Figure 13: **Comparison of raw spatial maps using different backbones for CO-PATCH.** The spatial map becomes more fine-grained for the backbone with higher dimensions for the number of patches (7×7 in CLIP ViT-B/32; 14×14 in CLIP ViT-B/316; 16×16 in DFN ViT-H/14).

Surprisingly, simply negating the patch-level image embeddings before feeding them to the post-layer norm and multiplying them with the projection weight naturally resolves the opposite visualization and out-of-range issues. As shown in Figure 12, the correlation between values of $\mathcal{M}_{ij}^l = \cos(\tilde{E}_p^l[i, j], E_{\text{ConText}})$ (y -axis) and $\mathcal{M}_{\text{Neg}}^l = -\cos(E_p^l[i, j], E_{\text{ConText}})$ (x -axis) is positive ($\forall i, j = \{1, \dots, p\}$). This observation is a product of the definition of cosine similarity:

$$\cos(-x, y) = \frac{(-x) \cdot y}{\| -x \| \| y \|} = \frac{-(x \cdot y)}{\| x \| \| y \|} = -\cos(x, y)$$

This suggests that the feature negation can serve as a proxy for semantic opposition, providing an effective mechanism at a low cost for enhancing the model’s spatial reasoning. Our raw spatial map ($\mathcal{M}^l = (\mathcal{M}_{ij}^l)_{1 \leq i, j \leq p}$) can be found in Figure 13 across different backbones. The final interpolated, clustered spatial map, CoMap, using different exit layers can also be observed in Figure 14.

Method – Stage 2: Mask Selection via Clustered Context-Aware Spatial Map (CoMap). During the clustering process, our algorithm first creates a binary mask (\mathcal{B}) by thresholding the input

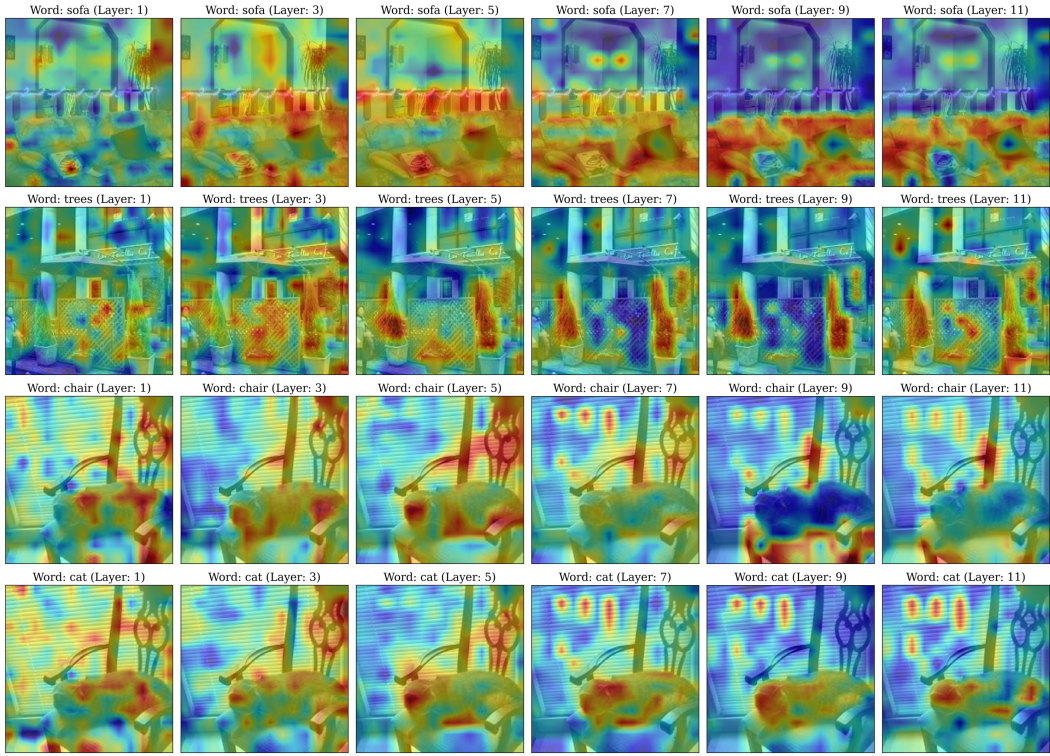


Figure 14: **Comparison of our spatial map, CoMap generated using varying exit layers.** Similar to the mIoU performance trend across different exit layers in Figure 9a, CoMap captures the most intuitive image-text similarity using the intermediate layers close the last layer (e.g., layer 9).

continuous spatial map (\mathcal{M}) to identify all relevant patches (line 1). An output cluster map (\mathcal{C}) is initialized with all zeros, and a counter (l) is also initialized to 0 (line 2). Then, each patch coordinate in the binary mask is iterated to find and assign a label to an unlabeled, active patch, which serves as the seed for a new cluster (lines 3-7). The algorithm then initiates a Breadth-First Search (BFS) from the seed, which continues as long as the queue (\mathcal{Q}) is not empty, to progressively label all patches belonging to the same connected component. Note that the number of automatically generated clusters from our CoMap (k) may differ per sample.

C ADDITIONAL RESULTS

Here, we explain results not shown in the main paper. All inference is conducted on a single RTX A4000 (16 Gi) for all the models with CLIP ViT-B/32 and ViT-B/16 backbones. For the DFN ViT-H/14 backbone, a single RTX A6000 (48 Gi) is used. To ensure a fair comparison for calculating the inference time in Table 4, we use the same device, RTX A6000, for all the methods.

C.1 SPATIAL MAP COMPARISON

Segmentation Approaches. Our final spatial map, CoMap, is surprisingly comparable to several zero-shot segmentation models, such as CLIPSurgery (Li et al., 2023) (Figure 15) and CLIP-Trace (Shao et al., 2024) (Figure 16). CLIPSurgery is generated via recomputation of the self-attention operation ($A = \sigma(s \cdot VV^T)V$ instead of $A = \sigma(s \cdot QK^T)V$, where s : scaling factor) for every layer (before the start of the new path). Similarly, CLIPTrace also requires a recomputation of self-attention for producing a more consistent semantic correlation matrix. However, CoMap does not require recomputations for self-attention modules and produces intuitive activation patterns similar to those of these segmentation models.

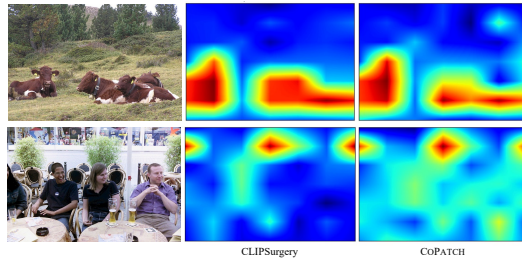


Figure 15: **Activation pattern comparison between CLIPSurgery and COPATCH.** Our spatial map shows a very similar activation as CLIPSurgery without attention recomputations.

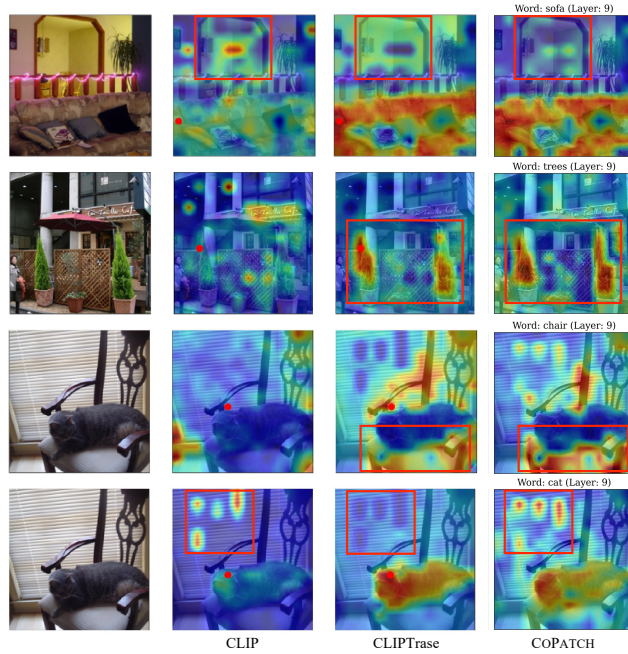


Figure 16: **Activation pattern comparison between CLIPTrace and COPATCH.** Although CoPATCH does not show completely clean activations without noises (red blobs on the last row), it can still capture highly activated areas like CLIPTrace.

	RefCOCOg		RefCOCO		RefCOCO+		Average	
	Time	mIoU	Time	mIoU	Time	mIoU	Time	mIoU
IterPRIMe Wang et al. (2025)	3.20	46.0	5.42	40.2	4.82	44.2	4.48	43.5
CoPATCH (CLIP ViT-B/32)	1.27	52.2	1.45	46.8	1.44	44.1	1.38	47.7
CoPATCH (CLIP ViT-B/16)	1.40	54.4	1.60	50.1	1.60	46.8	1.53	50.4
CoPATCH (DFN ViT-H/14)	2.24	56.2	2.52	50.9	2.53	47.1	2.43	51.4

Table 4: **Inference time and performance comparison between IterPRIMe and COPATCH on validation (U) sets.** We report the time in seconds per iteration, averaged across the first 100 samples for each dataset. Our methods comparatively take less time than IterPRIMe while achieving better IoU performance.

Grad-CAM. When compared to Grad-CAM (Selvaraju et al., 2016), which is often applied in several zero-shot RIS approaches (Subramanian et al., 2022; Wang et al., 2025; Lee et al., 2023a), Figure 17 demonstrates that our CoMap can provide better spatial cues for a primary object from a referring expression. Furthermore, our COPATCH (using CoMap) takes less inference time than IterPRIMe, which uses Grad-CAM, as shown in Table 4 while achieving better IoU performance.

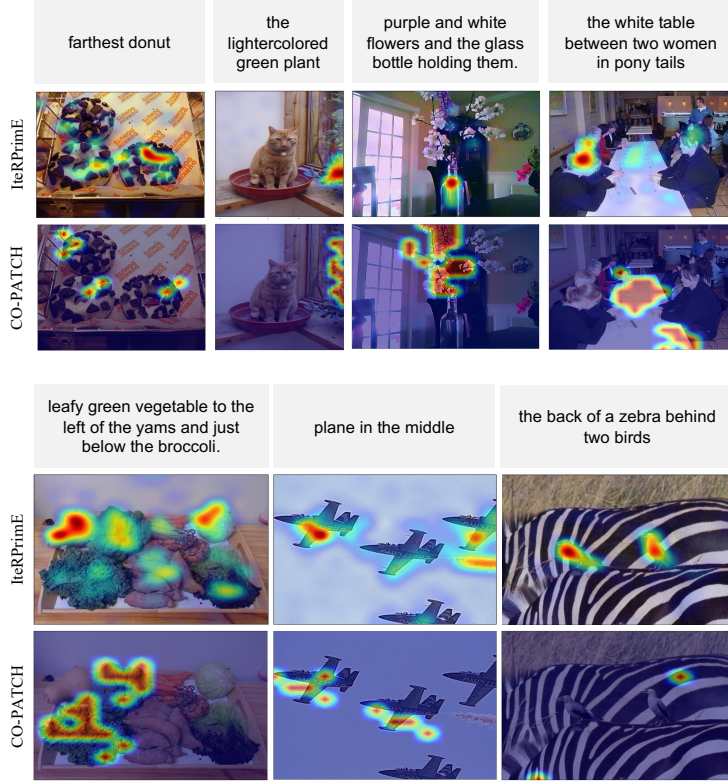


Figure 17: **Qualitative comparison between Grad-CAM (IteRPrimE) and CoMap (CO-PATCH).** Our CoMap can better capture and localize the primary objects in the referring expressions.

		FreeSOLO		SAM		Mask2Former	
		mIoU	oIoU	mIoU	oIoU	mIoU	oIoU
Global-Local (CLIP ViT-B/32)	Yu et al. (2023)	33.59	31.02	38.56	27.04	45.23	32.59
HybridGL (CLIP ViT-B/32)	Liu & Li (2025)	30.66	27.97	41.54	29.89	44.27	32.17
HybridGL [†] (CLIP ViT-B/16)		30.84	28.02	46.59	37.04	43.90	31.73
IteRPrimE (ALBEF)	Wang et al. (2025)	29.03	26.36	25.23	21.27	46.89	41.09
Mask Upper Bound (CLIP ViT-B/32)		52.44	52.76	74.39	75.76	76.85	72.73

Table 5: **Zero-shot performances of SoTA referring image extraction methods applied with three mask generators on RefCOCOg val (U) set.** The highest IoU performances are generally achieved using Mask2Former across different methods. [†] stands for the reproduced results.

	Pretrained Models	RefCOCOg			RefCOCO			RefCOCO+		
		val (U)	test (U)	val (G)	val	testA	testB	val	testA	testB
CoPATCH (CLIP ViT-B/32)	SAM	50.59	50.64	51.27	47.59	50.25	44.04	50.54	53.42	45.98
CoPATCH (CLIP ViT-B/16)	SAM	57.67	57.88	58.35	50.06	48.94	50.88	51.65	50.75	52.93

Table 6: **Zero-shot performances of SoTA referring image extraction methods applied with SAM on RefCOCOg val (U) set.** The highest IoU performances are generally achieved using Mask2Former (Table 1) across different backbones.

C.2 MASK GENERATOR SELECTION

For selecting the mask generator, we compare three widely used pretrained segmentation models, FreeSOLO (Wang et al., 2022a), SAM (Kirillov et al., 2023), and Mask2Former (Cheng et al., 2022; Liang et al., 2023) on several SoTA zero-shot RIS approaches (Yu et al., 2023; Wang et al., 2025; Liu & Li, 2025). As can be observed in Table 5, we observe that Mask2Former is most effective in

	Pretrained Models	RefCOCOg			RefCOCO			RefCOCO+		
		val (U)	test (U)	val (G)	val	testA	testB	val	testA	testB
Zero-shot methods (CLIP ViT-B/32)										
Global-Local Yu et al. (2023)	FreeSOLO	31.11	30.96	30.69	24.88	23.61	24.66	26.16	24.90	25.83
Global-Local Yu et al. (2023); Suo et al. (2023)	SAM	27.57	27.87	27.80	22.43	24.66	21.27	26.35	30.80	22.65
HybridGL [†] Liu & Li (2025)	SAM	36.16	36.27	36.16	32.02	32.50	31.98	29.73	31.75	26.64
TAS Suo et al. (2023)	SAM, BLIP-2	35.84	36.16	36.36	29.53	30.26	28.24	33.21	38.77	28.01
COPATCH (Top-1)	Mask2Former	41.43	41.98	41.37	37.17	44.63	31.53	35.15	43.14	29.97
COPATCH (Top-3)	Mask2Former	57.96	57.78	57.80	50.28	58.79	46.09	54.02	62.24	47.86
Zero-shot methods (CLIP ViT-B/16)										
Ref-Diff Ni et al. (2023)	SAM, SD	38.62	37.50	38.82	35.16	37.44	34.50	35.56	38.66	31.40
HybridGL Ni et al. (2023)	SAM	42.47	42.97	-	41.81	44.52	38.50	35.74	41.43	30.90
COPATCH (Top-1)	Mask2Former	44.13	46.24	45.26	40.85	48.45	34.98	38.39	46.17	32.15
COPATCH (Top-3)	Mask2Former	61.09	63.61	63.03	52.92	60.79	47.27	55.46	63.32	48.06
Zero-shot methods (DFN ViT-H/14)										
COPATCH (Top-1)	Mask2Former	46.21	46.03	46.09	41.24	48.88	36.15	38.10	45.11	33.14
COPATCH (Top-3)	Mask2Former	65.55	66.99	66.59	55.95	65.45	49.83	60.11	67.68	53.06

Table 7: **Comparison of oIoU performances across zero-shot RIS methods on RefCOCOg, RefCOCO, and RefCOCO+ datasets.** We attain the overall best performances for CLIP (ViT-B/32 and ViT-B/16) and DFN (ViT-H/14), outperforming the SoTA, TAS Suo et al. (2023), and HybridGL Liu & Li (2025). Note that we [†] stands for the reproduced results.

the RefCOCOg validation (U) set (Mao et al., 2016). Compared to SAM, it is also highly efficient, taking a fifth of the inference time (e.g., 150 min. vs. 30 min. using SAM and Mask2Former on 2,573 data instances) while mostly achieving higher IoU performances across different methods and similar upper bound scores (e.g., mIoU of 74.39 and 76.85 using SAM and Mask2Former, respectively). We also report the results of our COPATCH using SAM in Table 6.

C.3 oIoU PERFORMANCE

Table 7 shows the oIoU performances of various zero-shot RIS methods, including ours, across RefCOCO datasets. Similar to the mIoU results, COPATCH achieves the best overall results for all the backbones. Notably, COPATCH (CLIP ViT-B/32) achieves oIoUs of 41.98, 44.63, and 43.14 in RefCOCOg, RefCOCO, and RefCOCO+ test sets, which are +5.82p, +14.37p, and +4.37p higher than the previous SoTA method, TAS (Suo et al., 2023).

C.4 QUALITATIVE COMPARISON

Additional qualitative results of comparing Global-Local (+CT) and COPATCH (top-1) are illustrated in Figures 18 and 19. While Figure 18 shows several samples that our approach accurately segments by predicting the top-1 candidate mask correctly, Figure 19 shows several challenging cases even using our approach. For example, the first row sample in Figure 19 is segmented on the ‘the first half of the sandwich to the ‘right’ instead of ‘left.’ for top-1 and top-3 predictions of COPATCH. Despite this, the top candidate masks produced using our method are much diverse compared to those produced using the Global-Local method Yu et al. (2023).

C.5 CONTEXT TOKEN EFFECT

We also show qualitative results of the effects of our context tokens on the segmented results in Figure 20. We highlight the context tokens in red that are added as the local-level features of the hybrid text features described in Section 3.1. As noted, the model could better predict the primary object from the referring expression, given the context of colors. For instance, the fourth sample in Figure 20 guides a model to locate the bike nearest to the ‘green’ helmet. The last sample also corrects the model to focus on the ‘black’ property more than the woman wearing a dark navy jacket. We leave as future work to discover which of the context tokens within the referring expression could better guide the model for zero-shot RIS tasks.

C.6 SPATIAL SUBSET GENERATION

The prompt for instructing Qwen2.5-14B-Instruct (Yang et al., 2024) to classify each referring expression into ‘Spatial’ or ‘Non-Spatial’ depending on the presence of a spatial cue is in Table 8.

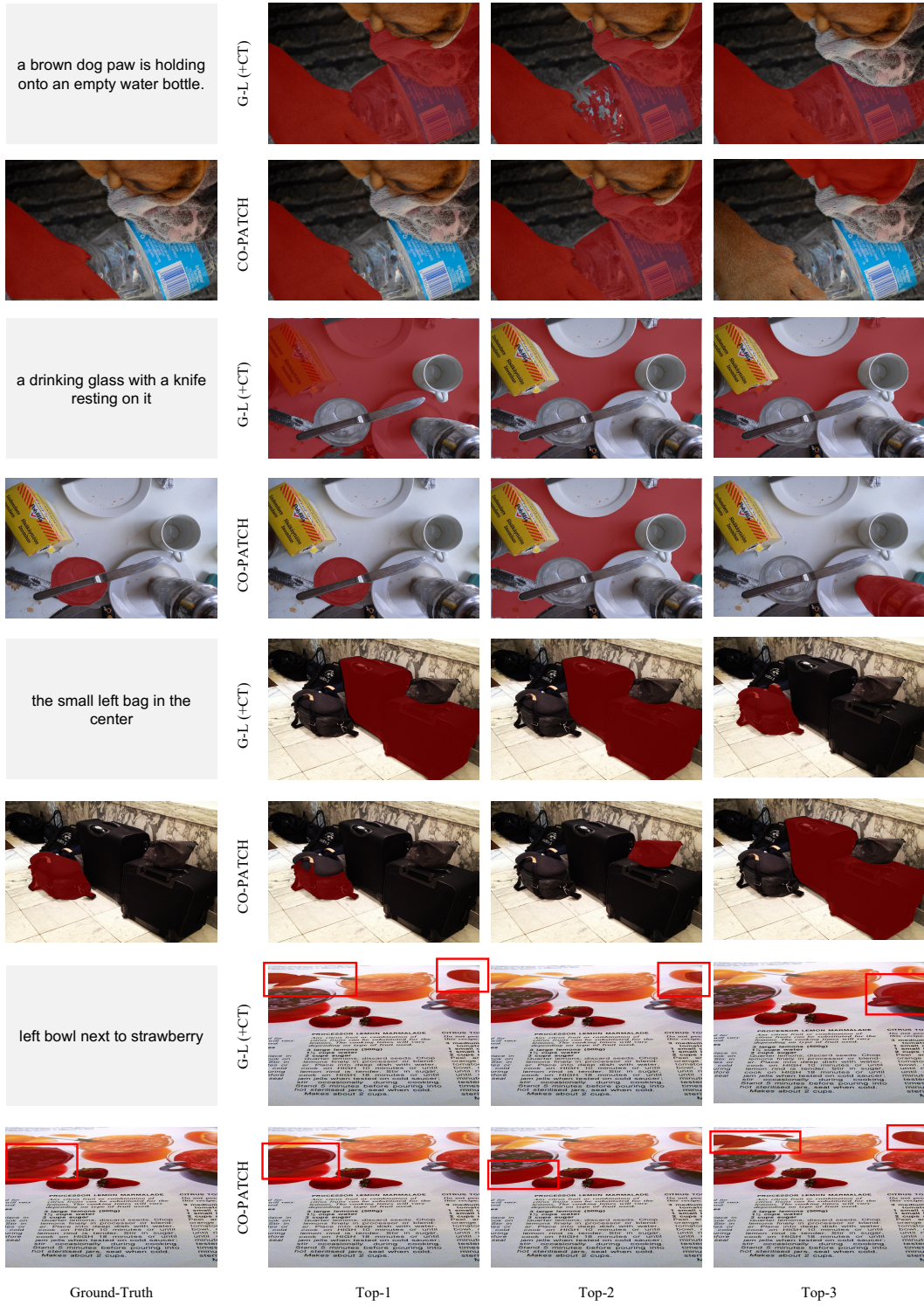


Figure 18: **Qualitative comparison of top candidate masks generated using original image-text similarity from Global-Local (w/ CT) and averaged CoMap similarity score using our Co-PATCH.** The top candidate masks generated using our method are much more diverse and accurate.

We provide important clarifications for the model to distinguish words that have multiple definitions

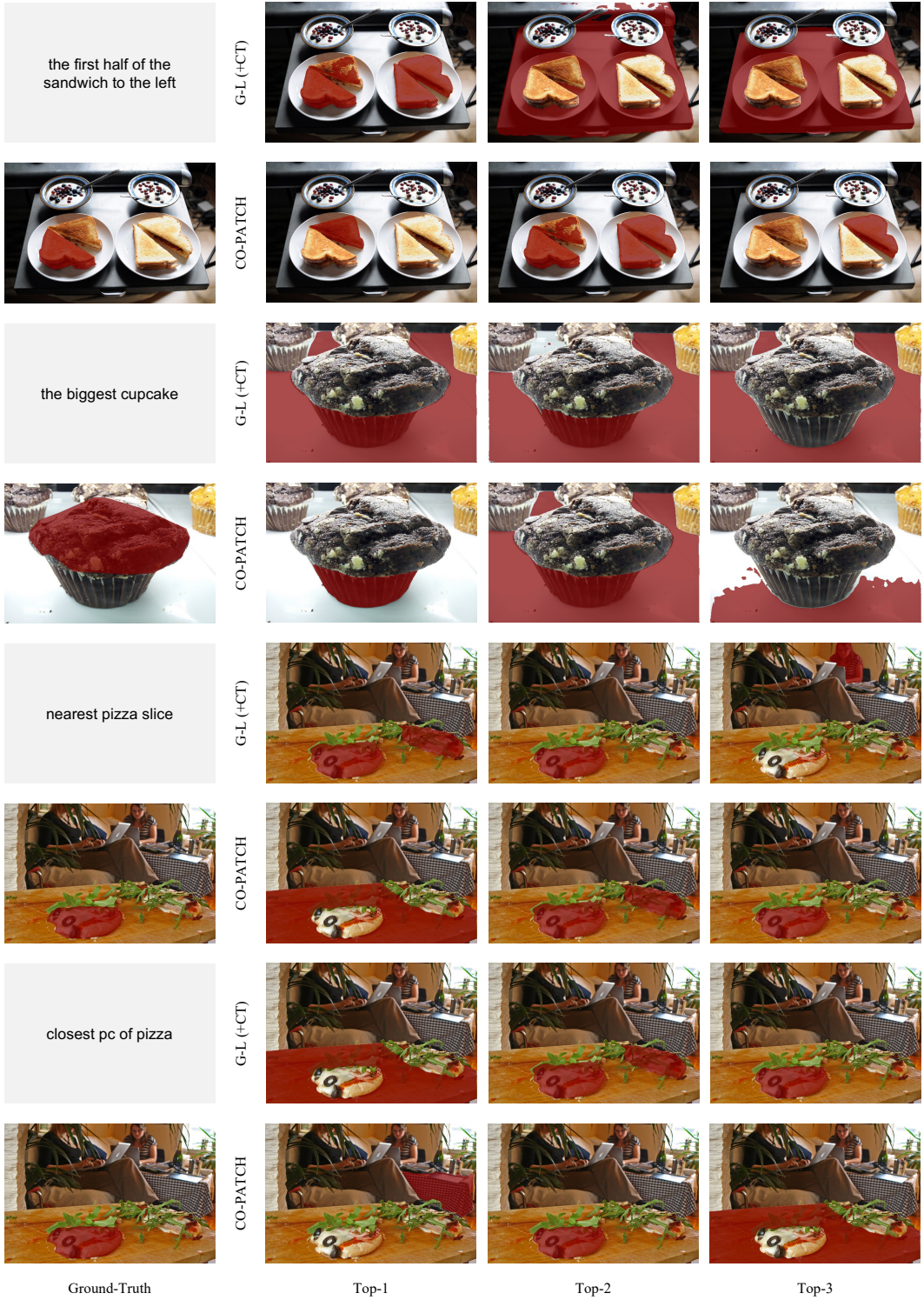


Figure 19: **Qualitative comparison of top candidate masks generated using original image-text similarity from Global-Local (w/ CT) and averaged CoMap similarity score using our CoPATCH.** The top candidate masks generated using our method are much more diverse.

(e.g., right, in) and several examples for classification. The list of unique spatial cues ($n = 950$) found using LLM for all the RefCOCOg, RefCOCO, RefCOCO+ validation datasets is as follows¹:

¹Due to the space limit, we provide the first 173 cues only.

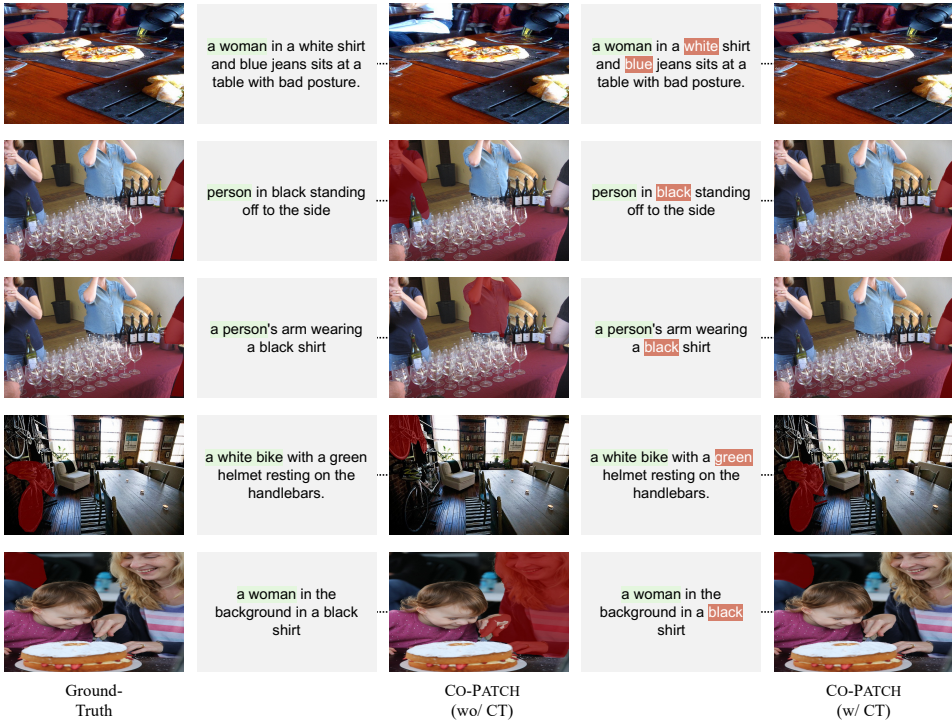


Figure 20: **Qualitative comparison between CO-PATCH without and with context tokens (CT).** We observe an improved mask candidate using hybrid text features highlighted with proposed context tokens in the local-level text features.

‘12 o’clock’, ‘2nd from’, ‘2nd from bottom’, ‘3rd from bottom’, ‘3rd one from’, ‘None.’, ‘above’, ‘above left of’, ‘above right’, ‘above, left of’, ‘above, on, right’, ‘above, right’, ‘above, right of’, ‘across’, ‘adjacent to’, ‘after’, ‘against’, ‘against, on top of’, ‘ahead of’, ‘alongside’, ‘amongst’, ‘around’, ‘around it’, ‘at’, ‘at 4 o’clock’, ‘at 9 o clock’, ‘at the edge of’, ‘at the end of’, ‘at the end of, on the left’, ‘atop’, ‘attached to’, ‘back’, ‘back behind’, ‘back end of’, ‘back end of, on, right edge of’, ‘back end... front’, ‘back from the right’, ‘back left’, ‘back left of’, ‘back middle’, ‘back of’, ‘back of chair center top’, ‘back of the chair on the right’, ‘back of the pack’, ‘back of the room right side’, ‘back of, closest to’, ‘back of, far right’, ‘back of, flanking it’, ‘back of, in front of’, ‘back of, in the middle, behind’, ‘back of, left’, ‘back of, on, left’, ‘back on right’, ‘back on the right’, ‘back right’, ‘back right top’, ‘back row 4th from left’, ‘back row on left’, ‘back side’, ‘back side position’, ‘back top almost middle’, ‘back up high’, ‘back, in the front of’, ‘back, on’, ‘back, right’, ‘back, to the right’, ‘back... right’, ‘background’, ‘background center’, ‘background, far left’, ‘background, on’, ‘background, top left’, ‘backleft’, ‘backside’, ‘behidn’, ‘behind’, ‘behind and right of’, ‘behind middle’, ‘behind right of’, ‘behind right side’, ‘behind, front’, ‘behind, in, middle’, ‘behind, in, near’, ‘behind, left’, ‘behind, left of’, ‘behind, left shoulder of’, ‘behind, next to’, ‘behind, next to, on’, ‘behind, on the right’, ‘behind, on, left’, ‘behind, on, left side’, ‘behind, on, left, near’, ‘behind, right’, ‘behind, right side’, ‘behind, to the left of’, ‘below’, ‘below, above’, ‘below, in’, ‘below, left’, ‘below, on, left’, ‘beneath’, ‘beneath, on’, ‘beside’, ‘beside, closest to’, ‘beside, in front of’, ‘between’, ‘between, on’, ‘between, on the right’, ‘between, on, bottom left of’, ‘between, on, right’, ‘blocked by’, ‘blocking’, ‘bottom’, ‘bottom center’, ‘bottom from top’, ‘bottom front’, ‘bottom front left’, ‘bottom left’, ‘bottom left area’, ‘bottom left corner’, ‘bottom left corner of’, ‘bottom left of’, ‘bottom left portion of couch on left’, ‘bottom left side’, ‘bottom left, on’, ‘bottom leftcorner’, ‘bottom middle’, ‘bottom most’, ‘bottom most left’, ‘bottom of’, ‘bottom portion of it’, ‘bottom right’, ‘bottom right corner’, ‘bottom right corner of pic’, ‘bottom right front’, ‘bottom right next to’, ‘bottom right of’, ‘bottom right on’, ‘bottom right under’, ‘bottom rightcorner’, ‘bottom rightmost’, ‘bottom row’, ‘bottom row 2nd from left’, ‘bottom row second from left’, ‘bottom row second kid from left’, ‘bottom row, left’, ‘bottom to right’, ‘bottom, 2nd from top’, ‘bottom, first row, closest to’, ‘bottom, left’, ‘bottom, on, top, left’, ‘bottom-left’, ‘bottom-right’, ‘bottom-right’,

System and User Prompts for Spatial Subset Generation

You are Qwen, created by Alibaba Cloud.

You are a helpful assistant.

Please carefully analyze user sentences to see if they contain spatial words or phrases.

Spatial expressions are any words or phrases indicating location, direction, orientation, or proximity.

These include (but are not limited to): ‘on’, ‘in’ (meaning ‘inside’), ‘under’, ‘front’, ‘behind’, ‘middle’, ‘center’, ‘left’, ‘right’ (direction), ‘closest to’, ‘near’, ‘beside’, ‘above’, ‘below’, ‘next to’, etc.

Important clarifications:

- If ‘right’ means ‘correct’, it is NOT spatial.
- If ‘in’ means ‘wearing’ (e.g., ‘in a costume’), it is NOT spatial.
- Action expressions like ‘facing’, ‘looking up’ is NOT spatial.
- ‘closest to’, ‘near’, or ‘middle’ should be treated as spatial. Respond with a specific format so it is easy to parse.’

Below are examples of how to classify:

Example 1:

Sentence: “The chair with the stuffed animal owl sitting in it.”

Analysis: ‘in’ here is adverb.

Answer: IsSpatial: False, SpatialExpression: None

Example 2:

Sentence: “The apple is on the table.”

Analysis: ‘on’ indicates spatial.

Answer: IsSpatial: True, SpatialExpression: on

Example 3:

Sentence: “left side monitor”

Analysis: ‘left’ indicates spatial.

Answer: IsSpatial: True, SpatialExpression: left

Example 4:

Sentence: “A small lamb lying closest to the adult.”

Analysis: ‘closest to’ indicates a spatial relationship.

Answer: IsSpatial: True, SpatialExpression: closest to

Now, analyze this new sentence:

{sentence}

Instructions:

- 1) If the sentence contains any spatial relationship expression, output True and the exact expression (e.g., ‘on’, ‘in’, ‘closest to’). Important: actions or wearing attributes are NOT spatial expression. (e.g. a girl facing the camera. -‘facing’ is NOT means direction or spatial relationship)
- 2) If no spatial expression is found, output False and None.
- 3) Return your answer in the format exactly: “IsSpatial: ;True/False;”, SpatialExpression: ;expression or None;”

Table 8: **Prompts used for generating spatial subsets of RefCOCO, RefCOCO+, and RefCOCOg validation sets.** We prompt Qwen2.5-14B-Instruct to divide the samples into Spatial and Non-Spatial subsets.

closest to’, ‘bottom/center’, ‘bottomright’, ‘by’, ‘by the wall’, ‘by the, on, left’, ‘by, with, to’, ‘center’, ‘center directly in front of’, ‘center front’, ‘center left’, ‘center leftish’, ‘center of’, ‘center of pic’, ‘center right’, ‘center row far right’, ‘center, behind’, ‘center/background’, ‘centermost’, ‘centernearest’.

C.7 HYPERPARAMETER TUNING

We show hyperparameter tuning results for CoPATCH (CLIP ViT-B/32) and CoPATCH (DFN ViT-H/14) in Figures 21 and 22, respectively. Similar to CoPATCH (CLIP ViT-B/16) results, the IoU

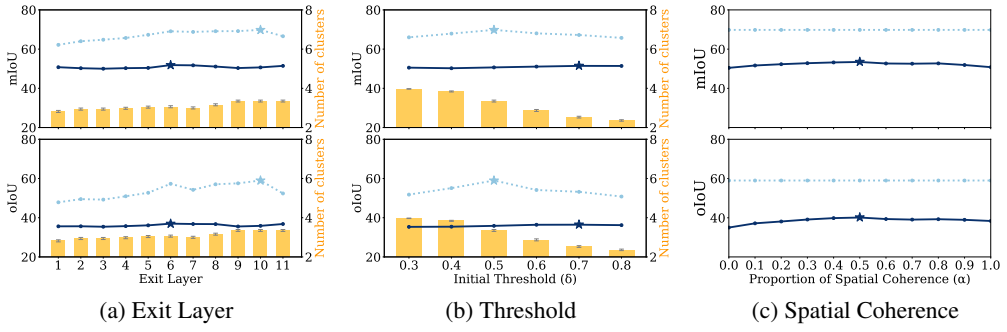


Figure 21: **Hyperparameter tuning results for COPATCH (ViT-B/32) using 10% of the Ref-COCOg val set.** The **deep-blue** and **sky-blue** lines depict **top-1** and **top-3** performances across exit layers. The **golden** bars represent the number of clusters averaged across data instances for each exit layer. We set the exit layer, initial threshold, and spatial coherence proportion to be 10, 0.5, and 0.5.

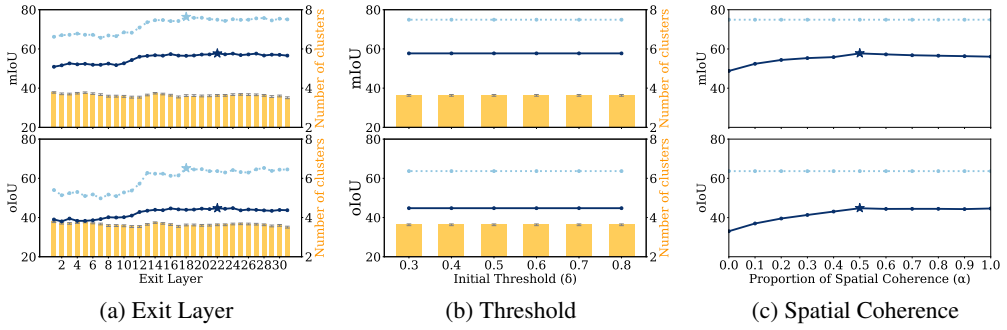


Figure 22: **Hyperparameter tuning results for COPATCH (ViT-B/32) using 10% of the Ref-COCOg val set.** The **deep-blue** and **sky-blue** lines depict **top-1** and **top-3** performances across exit layers. The **golden** bars represent the number of clusters averaged across data instances for each exit layer. We set the exit layer and spatial coherence proportion to be 22 and 0.5. Since the performance does not change depending on the initial threshold, we set it to the default setting ($\delta = 0.5$).

performances are not particularly sensitive to certain hyperparameter values. We select the exit layer (l) towards the last layer, yielding the best top-1 and top-3 performances. That means, for COPATCH (CLIP ViT-B/32) and COPATCH (DFN ViT-H/14), we select the 10-th (> 6) and 22-th (> 18) exit layer with the highest top-3 and top-1 performances. We select the initial threshold (δ) based on the top-3 performance for all three models. Lastly, since CoMap is not affected by the proportion of spatial coherence (α), α is selected based on the top-1 performance. We set the exit layer, initial threshold, and spatial coherence proportion to be 8, 0.3, and 0.7 for COPATCH (CLIP ViT-B/16) for all the performance results throughout the paper.

Note that the average number of clusters is not affected by the exit layer. However, it intuitively decreases as the initial threshold increases, only for COPATCH (CLIP ViT-B/16) and COPATCH (CLIP ViT-B/32). COPATCH (DFN ViT-H/14) is possibly less influenced due to the increased patch number (16) (see visualizations in Figure 13).

C.8 ALTERNATIVE TEXT FEATURE FUSION METHODS

We construct hybrid text features based on a weighted sum of global- and local-level text features, following previous works Yu et al. (2023); Liu & Li (2025). Here, we show results using an alternative fusion strategy of combining the features at an attention-level. Specifically, instead of merging the text features at the final layer, we encode the sentence-level (global) and primary noun and context token-level (local) text features separately until the fusion layer and merge the attention outputs

Method	Fusion Layer	RefCOCOg (oIoU / mIoU)	RefCOCO (oIoU / mIoU)	RefCOCO+ (oIoU / mIoU)
ATTN	1	31.65 / 42.07	34.57 / 41.05	36.32 / 41.89
ATTN	2	33.33 / 43.73	36.11 / 43.96	36.69 / 42.77
ATTN	3	24.80 / 35.20	30.03 / 37.37	30.29 / 35.33
ATTN	4	31.36 / 43.89	34.29 / 41.39	34.01 / 39.71
ATTN	5	33.13 / 45.45	34.92 / 42.64	33.80 / 38.52
ATTN	6	35.47 / 49.12	36.24 / 44.01	35.82 / 41.65
ATTN	7	38.70 / 51.22	36.99 / 44.67	33.80 / 39.57
ATTN	8	38.65 / 51.05	35.62 / 45.15	36.09 / 44.65
ATTN	9	31.94 / 48.17	39.56 / 48.36	35.42 / 42.77
ATTN	10	35.37 / 50.52	35.35 / 44.05	35.56 / 43.32
ATTN	11	35.85 / 51.09	31.09 / 41.53	34.50 / 42.07
WS	–	39.07 / 51.22	36.46 / 45.35	35.63 / 43.73

Table 9: **Performance comparison between attention-based (ATTN) and weighted-sum-based (WS) fusion strategies across RefCOCOg, RefCOCO, and RefCOCO+ (10%) validation datasets.** We observe that the best performance is achieved using exit layers from the middle layers that are closer to the final layers for both fusion methods.

Exit Layer	Entire RefCOCOg (val) oIoU / mIoU	10% RefCOCOg (val) oIoU / mIoU	10% RefCOCO (val) oIoU / mIoU	10% RefCOCO (testB) oIoU / mIoU
1	36.00 / 47.20	37.60 / 51.59	35.64 / 43.97	28.46 / 36.89
2	36.75 / 47.59	38.07 / 52.51	36.04 / 44.41	28.94 / 37.17
3	37.02 / 47.95	38.20 / 52.94	34.01 / 42.96	29.48 / 38.45
4	36.59 / 48.18	37.64 / 52.20	33.47 / 41.93	30.53 / 40.36
5	37.17 / 48.60	37.84 / 52.50	32.64 / 40.57	31.15 / 41.00
6	37.52 / 49.21	38.83 / 52.90	34.75 / 42.69	31.56 / 43.35
7	38.45 / 50.62	38.90 / 52.97	37.02 / 45.39	31.37 / 42.47
8	39.09 / 51.14	38.65 / 52.81	38.41 / 48.90	30.99 / 41.66
9	38.77 / 51.02	37.85 / 52.62	38.96 / 48.05	30.45 / 40.63
10	39.07 / 51.22	38.46 / 52.98	36.46 / 45.35	29.28 / 40.21
11	39.63 / 50.61	37.81 / 52.09	34.89 / 44.30	31.09 / 41.53

Table 10: **Layer-wise performance trends on different types of datasets.** We observe that using middle-to-late layers near the final layer generally provides the most generalizable spatial and semantic information.

Model Type (BLIP)	RefCOCOg			RefCOCO			RefCOCO+		
	val (U)	test (U)	val (G)	val	testA	testB	val	testA	testB
Global-Local (+CT)	15.26	12.52	13.28	18.79	11.35	8.97	18.67	11.33	10.32
CoPatch (Top-1)	30.80	25.37	31.34	39.64	28.15	30.08	39.57	26.55	22.74
CoPatch (Top-3)	47.25	45.14	47.45	57.30	42.38	42.84	59.08	44.38	41.83

Table 11: **Performance of BLIP-based models on RefCOCOg, RefCOCO, and RefCOCO+ datasets.** We show our method can be applicable to non-CLIP-based VLM, achieving superior performance than the baseline - Global-Local (+CT).

(i.e., $\text{fused}_{attn} + \gamma \text{global}_{attn} + (1 - \gamma) \text{local}_{attn}$) before encoding them to construct the hybrid text features. Note that we use the fused features for the remaining layers after going through the fusion layer. As shown in Table 9 ($\gamma = 0.5$), we find that merging the text features as a weighted sum yields better performance in RefCOCOg.

C.9 EXIT LAYERS

Since the choice of exit layer is important, as it directly affects the overall quality of our spatial map, COPATCH, we show a performance change across different layers using the entire vs. 10% of the RefCOCOg (val) dataset, containing long, complex referring expressions, and 10% of the RefCOCO

(val), and RefCOCO (testB) datasets, which contain various objects of the same category per image in relatively shorter referring expressions (Yang et al., 2022). Although the most optimal exit layer slightly differs across the datasets, the selected exit layers per dataset/domain are mostly the middle layers near the final layers (6–11), as can be shown in Table 10.

C.10 GENERALIZABILITY TO NON-CLIP-BASED VLMs

We use CLIP variants for a fair comparison with previous zero-shot RIS methods. However, to demonstrate the applicability of our method to other types of VLM, we show the results of applying our method to the BLIP model Li et al. (2022b) using Mask2Former. Whereas the final mask is selected based on the similarity between the original image and text embeddings for the Global-Local Yu et al. (2023) (+CT; Context Token) method, our method selects the best mask from top candidates (TC), reranked using our CoMap. As can be observed in Table 11, using our method consistently shows performance improvement compared to the Global-Local method.

D DISCUSSION

D.1 LIMITATIONS AND FUTURE WORK

We provide limitations of our framework and suggest future research directions for zero-shot RIS.

Spatial Guidance. The current spatial guider does not always select the correct candidate among different top candidate masks, leading to a gap in top-1 and top- k IoU performances. Here, our goal is not to use any other additional models except for the pretrained CLIP backbone and mask generator. However, future work could explore an external spatial guide that can better select the final mask among the top candidate masks provided by our CoMap.

Spatial Map. The primary goal of this paper is to *provide spatial cues* for RIS tasks using the proposed spatial map, CoMap, using image embeddings extracted from intermediate layers. The current spatial map could serve as a baseline for *top candidate mask augmentation* to disperse the model’s attention to look into multiple target objects located in different positions. We leave as a future work to extend the application of the presented spatial map into segmentation tasks that often require more refined segmentation, possibly with additional postprocessing methods (Shao et al., 2024; Bai et al., 2024).

D.2 SOCIETAL IMPACT

The current study investigates zero-shot RIS, a task that requires a model to segment image regions based on free-form natural language descriptions—even for categories or concepts unseen during training. Without a need for additional training on explicit annotations, our method provides a flexible, adaptable approach to be applicable to many tasks related to spatial understanding. This zero-shot RIS system has the potential to significantly reduce reliance on costly human workers, paving the way for broader, scalable deployment An et al. (2023); Lee et al. (2023b); An et al. (2024; 2025b). For instance, in healthcare, zero-shot RIS could aid radiologists to highlight specific regions of interest in medical scans (e.g., “the slightly darkened area near the lower part of the left lung”) for detailed examination. Applying zero-shot RIS to recent advanced fields could enhance the effectiveness and accessibility of vision-language systems involving precise interpretation of free-form user input of referring expressions.

D.3 ETHICAL AND REPRODUCIBILITY STATEMENT

Our work aims to leverage pretrained CLIP to improve general-purpose zero-shot RIS performance. The unintended bias may occur from the pretrained model itself; however, a comprehensive analysis and mitigation of such biases are beyond the scope of this work, which focuses on the core segmentation task. We provide data and code in the supplementary materials to ensure the reproducibility of our research.